Title:

Infarct Evolution in a Large Animal Model of Middle Cerebral Artery Occlusion

Authors:

*Mohammed Salman Shazeeb[1,2] (Corresponding author)
*Robert M. King[1,3]
Olivia W. Brooks[1,4]
Ajit S. Puri[1]
Nils Henninger[5,6]
Johannes Boltze[7]
Matthew J. Gounis[1,2]

[1]New England Center for Stroke Research, Department of Radiology
University of Massachusetts Medical School, Worcester, MA, 01655, USA.

[2]Image Processing and Analysis Core, Department of Radiology
University of Massachusetts Medical School, Worcester, MA, 01655, USA.

[3]Department of Biomedical Engineering
Worcester Polytechnic Institute, Worcester, MA, 01609, USA.

[4]St. George's University School of Medicine, Grenada, West Indies

Departments of [5]Neurology and [6]Psychiatry
University of Massachusetts Medical School, Worcester, MA, 01655, USA.

[7]University of Warwick, School of Life Sciences, Coventry, CV4 7AL, United Kingdom

*These authors contributed equally to this work

Corresponding address:

Mohammed Salman Shazeeb, Ph.D.
Department of Radiology
Division of Biomedical Imaging and Bioengineering
University of Massachusetts Medical School
55 Lake Avenue North, S7-410, Worcester, MA 01655, USA
E-mail: Mohammed.Shazeeb@umassmed.edu
Phone: 508-856-4255
Fax: 508-856-6363

Sources of funding: Dr. Henninger is supported by K08NS091499 from the National Institute of Neurological Disorders and Stroke (NINDS) of the National Institutes of Health (NIH). The content is solely the responsibility of the authors and does not necessarily represent the official views of the NIH. Dr. Gounis has received research support from the NIH, the United States – Israel Binational Science Foundation, Anaconda, Cerenovus, Ceretrieve, Cook Medical, Gentuity, Imperative Care, InNeuroCo, Magneto, Microvention, Medtronic Neurovascular, MIVI Neurosciences, Neuravi, Neurogami, Philips Healthcare, Rapid Medical, Route 92 Medical, Stryker Neurovascular, Syntheon, and the Wyss Institute.

Running headline: Infarct Evolution in a Canine Stroke Model

Abstract

Mechanical thrombectomy for the treatment of ischemic stroke shows high rates of recanalization; however, some patients still have a poor clinical outcome. A proposed reason for this relates to the fact that the ischemic infarct growth differs significantly between patients. While some patients demonstrate rapid evolution of their infarct core (fast evolvers), others have substantial potentially salvageable penumbral tissue even hours after initial vessel occlusion (slow evolvers). We show that the dog middle cerebral artery occlusion model recapitulates this key aspect of human stroke rendering it a highly desirable model to develop novel multimodal treatments to improve clinical outcomes. Moreover, this model is well suited to develop novel image analysis techniques that allow for improved lesion evolution prediction; we provide proof-of-concept that MRI perfusion-based time-to-peak maps can be utilized to predict the rate of infarct growth as validated by apparent diffusion coefficient derived lesion maps allowing reliable classification of

dogs into fast versus slow evolvers enabling more robust study design for interventional research.

Key words: dog, middle cerebral artery occlusion, infarct growth rate, perfusion MRI, time-to-peak, stroke.

Introduction

In recent years, randomized-controlled trials have shown that mechanical thrombectomy is a highly effective treatment for selected ischemic stroke patients with emergent large vessel occlusion (ELVO) [1-3]. Although clinical trials and uncontrolled stroke registries report successful recanalization of the primary artery in approximately 85% [4, 5], rates of good clinical outcomes have not yet matched the high rate of technical success. For this reason, novel approaches to multimodal intervention that includes neuroprotection, adjunctive technology to augment brain perfusion, thrombolysis, and recanalization with thrombectomy promise to maximize the probability of a good clinical outcome after ELVO. In particular, methods that can slow infarct progression may expand the availability of mechanical thrombectomy for ELVO patients that present beyond established treatment windows [6, 7]. Approaches under development include transient aortic occlusion [8], stimulation of circle of Willis nerve fibers [9], mild induced hypertension [10], and inhalation of nitric oxide [11]. Perhaps the greatest opportunity is re-exploration of pharmacological neuroprotection combined with mechanical thrombectomy [12-15].

Although multiple animal stroke models are available in a variety of species to study stroke pathophysiology and possible treatment modalities [16], only larger animal species such as rabbits [17], non-human primates [18, 19], and dogs [20-27] are suitable for creating ELVO via an endovascular approach without performing a craniotomy. However, to date only the dog model allows simulation of mechanical thrombectomy for ELVO [28]. Moreover, the gyrencephalic brain of dogs renders it structurally and functionally more similar to the human brain than that of rodents [29]. Unlike sheep [30,

31] and swine [32], dogs do not possess a *rete mirabile*, thus allowing direct endovascular access to the middle cerebral artery (MCA) for creating an occlusion as well as achieving mechanical recanalization [28, 33, 34]. The dog ELVO model has been developed to allow for the assessment of neuroprotectants and other novel therapeutics [35]. Prior studies suggested that the dog model may be limited by its variable ischemic lesion evolution possibly due to irregular collateral circulation [36, 37]. Here we formally explored the possibility that this variability is similar to the human condition and contributes to the different rates of infarct evolution [38]: 1.) fast progressors, who experience rapid infarct growth with a large ischemic core and failing collaterals despite an early diagnosis within 6 h of stroke onset [39, 40]; and 2) slow progressors, who experience slow infarct growth maintaining a small ischemic core and good collaterals with significant salvageable tissue beyond the 6 h time window [41, 42].

Diffusion- (DWI) and perfusion-weighted imaging (PWI) are common magnetic resonance imaging (MRI) techniques used for diagnosing ischemic stroke in the clinical setting [43-49]. The DWI-derived apparent diffusion coefficient (ADC) of cerebral tissue decreases within the region of the irreversibly injured infarct core that can be detected using appropriate thresholds [50-52]. Several PWI parameters derived from dynamic susceptibility contrast (DSC)-MRI including cerebral blood flow (CBF), cerebral blood volume (CBV), mean transit time (MTT), time of maximum value of the tissue residue function (Tmax), bolus arrival time (BAT), and time-to-peak (TTP) concentration become altered as normal cerebral tissue progresses from ischemia to infarction [53]. The DWI/PWI mismatch has been used to predict the extent of infarction and identify patients likely to benefit from reperfusion therapy [54, 55]. However, depending on the PWI

parameter used and the method implemented to compute it, studies have reported an inconsistency in the identification of the final infarct volume especially when using parameters like CBF and MTT [53, 56-68]. On the other hand, PWI parameters like Tmax and TTP have been shown to more accurately estimate the final infarct size [54, 69-77].

The DEFUSE 2 clinical trials reliably showed that patients with target mismatch (based on Tmax thresholds) who underwent early reperfusion after endovascular stroke treatment had more favorable clinical outcomes compared to patients without target mismatch [78]. In a previous dog ELVO model an infarct growth model was developed to predict the infarct growth rate and final infarct volume based on DWI lesion volume and pial collateral quantification from computed tomography (CT) angiograms [37]. However, this model was based on fast evolvers and thus it is uncertain whether results can be translated to slow evolvers. The ability to differentiate fast from slow evolvers early on is an important issue to minimize bias in studies utilizing the dog model to assess novel treatment approaches. To address this issue, we leveraged the presence of slow versus fast evolving ischemic lesions in our established dog ELVO model to predict the infarct evolution using PWI-based TTP maps, derived from DSC-MRI, based only on the first PWI image acquired after the onset of stroke. Correct classification of the infarct evolution from study inception has the advantage to exclude one type of progressor or to prospectively enter animals into appropriate cohorts in therapeutic studies, thereby increasing the scientific rigor.

Materials and Methods

Animal preparation

All animal research procedures were performed as approved by the Institutional Animal Care and Use Committee (IACUC) of the University of Massachusetts Medical School (Worcester, MA, USA). Fourteen purpose-bred dogs (8 females and 6 males; weight: 8.2–23.9 kg; age: 6.5–36 months) were used in this study. Details of the subject demographics are provided in Table 1. On the day of surgery, the animals were sedated and pre-treated with a single dose of intramuscular acepromazine (0.06 mg/kg), buprenorphine (0.02 mg/kg), and glycopyrrolate (0.01 mg/kg). Anesthesia was induced with an intravenous dose of propofol (3–4 mg/kg), and the animal was intubated. Anesthesia was maintained by mechanical ventilation with 1–3% isoflurane in air. Throughout anesthesia, animals were monitored by electrocardiogram (ECG), peripheral capillary oxygen saturation (spO_2), invasive or non-invasive arterial blood pressure, rectal temperature, and end-tidal CO_2. All vital measurements were maintained within the physiological range [79]. Using a modified Seldinger technique, an 8F hemostatic introducer was placed in the right femoral artery to allow endovascular access and blood draw for preparing blood clots as previously described in detail [28]. A 6-french Navien-072 catheter (Medtronic Neurovascular, Irvine, CA) was navigated under fluoroscopic guidance to the origin of the right or left internal carotid artery (ICA), at which point an autologous clot [28] was injected and advanced to permanently occlude the MCA (Fig. 1). The side of clot injection was selected on the basis of the larger diameter and length of non-tortuous cervical ICA for delivery of this relatively large catheter.

Imaging protocol

Once correct clot placement at the origin of the MCA was confirmed by fluoroscopy (Allura Xper FD20; Philips Healthcare, Best, the Netherlands), the animal was transferred

to the MRI scanner (Phillips Achieva/Phillips Ingenia 3T, Philips Healthcare), which is physically adjacent to the angiography suite. An 8-channel knee coil (Philips Healthcare) was used to acquire the brain scans. The imaging protocol included time-of-flight (ToF) imaging (TR/TE 20/4 ms, FA = 20^{o}, matrix 332 × 212), DWI (TR/TE 2600/76 ms, FA = 90^{o}, b-value = 0, 1000 s/mm^{2}, NSA = 6, matrix 144 × 144), PWI (TR/TE 1500/20.1 ms, FA = 40^{o}, 60 dynamics, matrix 320 × 320), and T2-weighted (T2W)-FLAIR imaging (TR/TE 11000/125 ms, TI 2800 ms, FA = 90^{o}, ETL = 27, matrix = 288 × 288). FLAIR imaging was used to rule out the possibility of subarachnoid hemorrhage. For PWI, 0.2 mmol/kg of gadopentetate dimeglumine (Magnevist, Bayer Healthcare Pharmaceuticals, Leverkusen, Germany) was injected intravenously (IV) after the second of 60 dynamic scans (total scan time = 90 s), followed by 15 ml saline bolus. DWI was obtained approximately every half hour up to 4.5 h post-clot injection. To calculate the infarct core volume, ADC maps were generated from the DWI images. Once the final diffusion image was acquired, the animal was euthanized, and in selected cases the brain was harvested immediately for histological assessment to confirm the final infarct size.

Image analysis

In order to assess the rate of infarct evolution based on DWI images, ADC maps were generated using MATLAB (The Mathworks, Inc., Natick, MA) and the datasets were binned in aggregates of 30 min. Since the goal of the study was to assess the rate of infarct evolution rather than the overall size of the infarct, the infarct size at each time-point was normalized by the final volume. When DWI was unavailable at a time point, linear interpolation was used to estimate the size of the normalized infarct.

Calculation of TTP maps was done offline using ImageJ (Rasband W. ImageJ. Bethesda, MD: http://rsb.info.nih.gov/ij/; 1997–2006) and MATLAB. The dynamic scans from PWI were used to segment the entire brain region in ImageJ. Scripts were written in MATLAB to calculate the TTP maps using the segmented brain slices from the dynamic scans on a voxel-by-voxel basis by locating the dynamic scan that contained the minimum intensity value. To obtain a relative TTP (rTTP) map, TTP maps were normalized by subtracting the mean TTP derived from a contralateral region of interest (ROI; positioned in the periventricular area of the unaffected hemisphere in the mid-brain region) from the absolute TTP in each voxel using the following equation:

$$rTTP_{map} = TTP_{map} - \frac{1}{n}\sum_{i=1}^{n}(ROI_{contralateral})_i$$

where *n* is the total number of voxels in the contralateral ROI.

To allow for exact voxel-wise analysis, all brain slices from the respective ADC and TTP maps were co-registered prior to analysis. This was accomplished by registering the B0 images from the DWI acquisition to the raw PWI images using a Dice similarity coefficient to confirm the best possible registration. This affine transformation was then applied to the ADC maps, which registered them to the rTTP maps. The areas defined as infarct on the final DWI were used to isolate only the voxels within the rTTP maps that ultimately evolved to infarction. The voxels on the rTTP maps were categorized into 4 bins: 4–8 s (slight delay), 9–13 s (moderate delay), 14–18 s (long delay), and 19+ s (extended delay). This categorization was used to predict the rate of infarct evolution using the rTTP maps and comparing them to the true rate of infarct evolution as measured using serial DWI. A summary of the image analysis is shown in Fig. 2. An rTTP infarct

evolution (rTTPIE) index was also calculated using the ratio of the rTTP map voxels in the extended delay and slight delay bins to quantify the rate of infarct evolution in fast and slow evolvers (Table 1). An rTTPIE index greater than 1 would indicate a fast evolver and less than 1 would indicate a slow evolver.

Final infarct determination

To minimize confounding of MRI to histology-determined infarct size, we used the ADC-thresholded core assessed on the final image set to determine final infarct volume, which has been previously shown to have a high correlation with TTC-based histology [80, 81]. In addition, we used a subset of animals to assess the final infarct volume histologically. Following extraction, brains were placed in a -80°C freezer for approximately 20 min and then cut into approximately 5-mm thick sections. Each section was stained with 2,3,5-triphenyltetrazolium (TTC) for final infarct volume assessment.

Statistical analysis

All statistical analyses were done in R (R Development Core Team (2018). R: A Language and Environment for Statistical Computing (Version 3.5.2) [Software]. Vienna, Austria: R Foundation for Statistical Computing. Retrieved from http://www.R-project.org). For demographic data, analysis of variance (ANOVA) was used to identify any differences between the slow and fast evolvers. The Pearson product–moment correlation coefficient was used to check for significance of the correlations between the infarct volumes of the DWI and PWI images. For the comparison between histograms of the two groups (slow and fast evolvers), a paired t-test was used. Fisher's exact test was used to examine the significance of association between the rTTP map and DWI categorization of fast and

slow evolvers, i.e. to identify the capability of the rTTP maps to predict the DWI results. A two-sided $p < 0.05$ was considered significant in all analyses. A *post-hoc* power analysis was also performed using $\alpha = 0.05$ to verify the statistical power of the significant differences between the fast and slow evolvers in this study using the G*Power software package [82].

Results

MCA occlusion

Embolic MCA occlusion was successfully induced in all animals (n = 14) as confirmed by digital subtraction angiography (Fig. 1a, b). The persistence of the MCA occlusion was confirmed by ToF-MRI (Fig. 1c) in each animal. None of the animals displayed any hemorrhagic transformation (data not shown).

Imaging characteristics of fast evolvers

Figure 3 depicts a representative animal (Animal #4 from Table 1) that was assigned to the fast evolver group (based on the DWI designation discussed below). A single coronal slice is shown indicating an area of restricted diffusion in the right MCA territory (Fig. 3a). The corresponding ADC map of the same slice shows a hypointense region indicating the extent of infarct with a lesion averaged ADC value of ~0.5×10^{-3} mm^2/s (Fig. 3b). The corresponding TTC-stained brain section shows concordance of the histology with the ADC-defined region of infarction (Fig. 3c). The rTTP map, corresponding to the ADC map, derived from PWI images is displayed using a pseudo-color map indicating the same infarct region (Fig. 3d). The color intensity of the voxels

indicates that the infarct area with an elevated intensity are at or above ~20 s. Images from DSA in the early (Fig. 3e) and delayed (Fig. 3f) phase indicate a lack of collaterals in the right hemisphere.

Imaging characteristics of slow evolvers

Figure 4 shows a representative animal (Animal #1 from Table 1) that was assigned to the slow evolver group (based on the DWI designation discussed below), which revealed a smaller lesion size compared to the fast evolver in Fig. 3. A single coronal slice is shown where the infarct region is visible as an area of restricted diffusion in the left hemisphere (Fig. 4a). The corresponding ADC map of the same slice shows a hypointense region indicating the extent of infarct with an ADC value of ~0.5×10^{-3} mm^2/s (Fig. 4b). The corresponding TTC-stained brain section confirms the ADC-defined region of infarct (Fig. 4c). The TTP map, corresponding to the slice from the ADC map, derived from PWI images is displayed using a pseudo-color map indicating the same infarct region (Fig. 4d). The color intensity of the voxels in the infarct area only have a slightly elevated intensity with only a few voxels above ~20 s, which is in contrast to the elevated intensities observed in the fast evolver (Fig. 3d). Images from DSA in the early (Fig. 4e) and delayed (Fig. 4f) phase highlight the impact of the collaterals in the left hemisphere.

Fast and slow evolver designation using DWI

Based on the normalized infarct volume as a function of time using DWI (Fig. 5a), animals were categorized to fast versus slow evolvers. After MCA occlusion, fast evolvers showed a constant growth in the ADC-thresholded infarct volume during the first 2 h at which point infarct growth plateaued to reach the final infarct size. Slow evolvers

demonstrated a relatively slow infarct core evolution in the first 2 h with a secondary more rapid constant growth occurring afterwards until the final infarct size was reached at approximately 4 h after MCA occlusion. Thus, animals displaying more than 50% of total infarct volume within 2 h were assigned to the fast evolver group and animals displaying less than 50% of the total infarct volume within 2 h were assigned to the slow evolver group. Based on this definition, each animal in this study was designated with an infarct evolution rate (Table 1). A comparison between the demographics (sex, age, and weight) of the fast and slow evolvers did not show any significant difference (Table 2). The vital measurements between the groups also did not show any significant difference (data not shown)

Prediction of fast versus slow evolvers using initial PWI

The correlation plot (Fig. 5b) shows the agreement of the infarct volumes between the final DWI image and the TTP map generated from the initial PWI images ($R^2 = 0.99$). Based on the relative number of voxels within the “slight delay” and “extended delay” categories, animals were classified into fast and slow evolvers (Fig. 5c): the respective cutoff marks to distinguish between slow and fast evolvers were ~34% for the “slight delay” and ~42% for the “extended delay” bins based on the minimal distance (halfway point) between the boundary points of each category. This classification was more apparent using the rTTPIE index, which demonstrated a significant difference between the fast and slow evolvers (Table 2). For the remaining bins, the fast and slow evolvers did not show a significant difference. This rTTP-based classification correctly predicted the DWI results of all fourteen animals ($p < 0.01$, Fishers exact test for classification). The *post-hoc* analyses for this study revealed the statistical power to exceed 0.99 for the

detection of differences between the fast and slow evolvers using the “slight delay” and “extended delay” bins, and the rTTPIE index.

Ex vivo infarct assessment and correlation with MRI

In a subset of dogs (n = 6: 4 fast evolvers and 2 slow evolvers) after euthanasia, the brain was removed to histologically quantify the infarct volume using TTC. Overall, there was an excellent correlation between the final ADC-thresholded and the TTC-defined infarct volume (R^2 = 0.99) with a slope of 0.96 (data not shown).

Discussion

During human ELVO, the rate of infarct growth is determined by a combination of factors such as genetic background, demographics, physiological parameters, and other conditions that may influence collateral blood flow and ischemic tolerance [5, 38]. A key finding of our study was that the dog ELVO model, similar to monkeys [19], is characterized by variability in the ischemic stroke evolution that closely mimics the clinical scenario [38]. This phenomenon, in conjunction with the ability to study endovascular approaches to recanalization, renders the dog ELVO model as highly relevant to study novel therapeutic approaches in interventional research. Importantly, we show that voxel-wise analyses of PWI images allow to predict whether animals were fast or slow evolvers already on the first PWI scan obtained approximately 30 min after MCA occlusion.

Perfusion is a critical biological mechanism that reflects the delivery of oxygen and essential nutrients to tissue via blood flow. MR-based PWI has the potential to measure brain perfusion in acute stroke subjects and provide treatment options that may

significantly affect the clinical outcome. DSC-MRI, compared to other PWI techniques like dynamic contrast-enhanced (DCE)-MRI and arterial-spin labeling (ASL), offers faster scan times to get a quick measurement of transit time with whole brain coverage, which can be critical in driving treatment decisions with a limited time window [83]. The deconvolved PWI parameters derived from DSC-MRI such as CBF, CBV, and MTT, have been considered to be more reliable in detecting tissue at risk of infarction due to the use of an arterial input function (AIF), which takes into account any variations in physiological and injection conditions [84, 85]. However, the AIF shape is susceptible to errors due to several factors such as motion artifacts and partial volume effects among others.[86, 87] Non-deconvolved PWI parameters derived from DSC-MRI such as TTP and BAT, on the other hand, do not require the measurement of an AIF and are derived directly from the tissue concentration time curve without any deconvolution.

TTP has been suggested to rapidly identify tissue at risk of infarction (penumbral tissue) and predict infarct size and growth in stroke patients [73, 75, 76, 88-91]. Thresholds of TTP delay (TTP > 4 s best identifying penumbral flow) [54, 72-76, 88, 92] were used to determine the volume of tissue that would become viable or that were at risk to progress to infarct. These TTP thresholds have been compared with ^{15}O-water positron emission tomography (PET) studies and validated using ^{15}O-water PET-derived CBF threshold of <20 ml/100 g/min, which serves as the “gold standard” for detecting penumbral tissue in ischemic stroke [57, 74-76, 92, 93]. In this study, we expanded the role of TTP maps to assess the *extent* of critically hypoperfused brain tissue as well as to predict the *rate* of infarct evolution.

TTP maps have been generated in several different ways in clinical and animal studies over the last couple of decades. TTP map calculations have mainly been reported using three different methods where: 1.) TTP was defined as the time difference in peak intensity and the BAT [85, 94]; 2.) TTP was defined as the time from bolus injection to peak intensity [53, 54, 76, 95]; and 3.) TTP maps were generated using a normalization by subtracting a mean contralateral ROI of the unaffected hemisphere [54, 71-73, 75]. Since the latter method using normalization of the TTP map reduces AIF dependency (by lowering variability due to factors such as injection rate, catheter size, and cardiac output among others) and performs as well as deconvolved parameters in infarct prediction [57, 85, 86, 96], we used rTTP maps in this study to perform the histogram binning.

Histogram binning of rTTP maps successfully classified the animals into fast and slow evolvers based on the infarct growth rate observed in the ADC maps. The “slight delay” and “extended delay” bins in the histogram clearly distinguished between the fast and slow evolvers, which is numerically evident using the rTTPIE index. Utilizing the rTTP map binning scheme promises to be useful in prospectively determining whether an animal will progress as a fast or slow evolver – a major advantage when studying novel therapeutics as it would allow to control for variability in infarct progression as part of the randomization scheme.

Limitations

One limitation from our analysis was that only two types of evolvers (fast and slow) were distinguishable using the rTTP analysis. If the rTTPIE index value equaled close to

one, then that would correspond to having approximately equal number of voxels in the “slight delay” and “extended delay” histogram bins of the rTTP maps, which would make it difficult to assign the animal as a fast or slow evolver. In that case, an “intermediate evolver” designation maybe more appropriate. The rTTP analysis to predict fast and slow evolvers was done retrospectively, which requires prospective confirmation of these preliminary findings. There was a notable variation in animal age and weight related to the different strains of dogs included into our retrospective analysis. However, we did not find any significant age and weight difference between fast and slow evolvers, assuaging concerns of major confounding and may in fact indicate broad applicability of our results. During the course of this proof-of-concept study, histology was not performed in all dogs for confirmation of the ADC thresholded infarct volume. However, in our past experience, the selected ADC threshold is highly concordant with histology [27, 28].

Conclusion

The canine model of embolic stroke resulting in the occlusion of the MCA results in both slow and fast infarct evolution. Preliminary evidence demonstrates that infarct evolution pattern can be determined immediately after clot placement using perfusion-weighted MRI. These data support more robust preclinical assessment of complex, multimodal acute stroke therapies.

Compliance with Ethical Standards

Conflict of Interest

Dr. Henninger is supported by K08NS091499 from the National Institute of Neurological Disorders and Stroke of the National Institutes of Health (NIH). The content is solely the responsibility of the authors and does not necessarily represent the official views of the NIH. Dr. Henninger serves on the advisory board of Omniox, Inc. and serves as consultant to Astrocyte Pharmaceuticals, Inc. Dr. Gounis has been a consultant on a fee-per-hour basis for Cerenovus, Imperative Care, Mivi Neurosciences, Phenox, Route 92 Medical, Stryker Neurovascular; holds stock in Imperative Care and Neurogami; and has received research support from the NIH, the United States – Israel Binational Science Foundation, Anaconda, Cerenovus, Ceretrieve, Cook Medical, Gentuity, Imperative Care, InNeuroCo, Magneto, Microvention, Medtronic Neurovascular, MIVI Neurosciences, Neuravi, Neurogami, Philips Healthcare, Rapid Medical, Route 92 Medical, Stryker Neurovascular, Syntheon, and the Wyss Institute. All authors declare that they have no potential conflicts of interest in regard to the research, authorship, and publication of this paper.

Ethical Approval

All animal research procedures were performed as approved by the Institutional Animal Care and Use Committee (IACUC) of the University of Massachusetts Medical School (Worcester, MA, USA). This article does not contain any studies with human participants performed by any of the authors.

Author Contribution Statement

The concept of study was developed by Matthew Gounis, Nils Henninger, Johannes Boltze, and Ajit Puri. Robert King and Matthew Gounis performed the animal experiments and collected the imaging data. Olivia Brooks performed data analysis. Mohammed Salman Shazeeb developed the image analysis pipeline, performed image analysis, and wrote the manuscript. Robert King also performed image analysis. Mathew Gounis, Nils Henninger, Johannes Boltze, and Robert King made significant edits to the manuscript for intellectual content. All authors read and approved the final manuscript.

Supplementary Information

None

References

1. Saver JL, Goyal M, Bonafe A, Diener HC, Levy EI, Pereira VM et al. Stent-retriever thrombectomy after intravenous t-PA vs. t-PA alone in stroke. N Engl J Med. 2015;372(24):2285-95. doi:10.1056/NEJMoa1415061.
2. Jovin TG, Chamorro A, Cobo E, de Miquel MA, Molina CA, Rovira A et al. Thrombectomy within 8 hours after symptom onset in ischemic stroke. N Engl J Med. 2015;372(24):2296-306. doi:10.1056/NEJMoa1503780.
3. Campbell BC, Mitchell PJ, Kleinig TJ, Dewey HM, Churilov L, Yassi N et al. Endovascular therapy for ischemic stroke with perfusion-imaging selection. N Engl J Med. 2015;372(11):1009-18. doi:10.1056/NEJMoa1414792.
4. Blanc R, Redjem H, Ciccio G, Smajda S, Desilles JP, Orng E et al. Predictors of the Aspiration Component Success of a Direct Aspiration First Pass Technique (ADAPT) for the Endovascular Treatment of Stroke Reperfusion Strategy in Anterior Circulation Acute Stroke. Stroke. 2017;48(6):1588-93. doi:10.1161/strokeaha.116.016149.

5. Mikati AG, Mandelbaum M, Sapnar S, Puri AS, Silver B, Goddeau RP, Jr. et al. Impact of Leukoaraiosis Severity on the Association of Time to Successful Reperfusion with 90-Day Functional Outcome After Large Vessel Occlusion Stroke. Transl Stroke Res. 2019. doi:10.1007/s12975-019-00703-0.
6. Bang OY, Goyal M, Liebeskind DS. Collateral Circulation in Ischemic Stroke: Assessment Tools and Therapeutic Strategies. Stroke. 2015;46(11):3302-9. doi:10.1161/strokeaha.115.010508.
7. Shuaib A, Butcher K, Mohammad AA, Saqqur M, Liebeskind DS. Collateral blood vessels in acute ischaemic stroke: a potential therapeutic target. Lancet Neurol. 2011;10(10):909-21. doi:10.1016/s1474-4422(11)70195-8.
8. Winship IR, Armitage GA, Ramakrishnan G, Dong B, Todd KG, Shuaib A. Augmenting collateral blood flow during ischemic stroke via transient aortic occlusion. J Cereb Blood Flow Metab. 2014;34(1):61-71. doi:10.1038/jcbfm.2013.162.
9. Henninger N, Fisher M. Stimulating circle of Willis nerve fibers preserves the diffusion-perfusion mismatch in experimental stroke. Stroke. 2007;38(10):2779-86. doi:10.1161/strokeaha.107.485581.
10. Shin HK, Nishimura M, Jones PB, Ay H, Boas DA, Moskowitz MA et al. Mild induced hypertension improves blood flow and oxygen metabolism in transient focal cerebral ischemia. Stroke. 2008;39(5):1548-55. doi:10.1161/strokeaha.107.499483.
11. Terpolilli NA, Kim SW, Thal SC, Kataoka H, Zeisig V, Nitzsche B et al. Inhalation of nitric oxide prevents ischemic brain damage in experimental stroke by selective dilatation of collateral arterioles. Circ Res. 2012;110(5):727-38. doi:10.1161/circresaha.111.253419.
12. Bratane BT, Cui H, Cook DJ, Bouley J, Tymianski M, Fisher M. Neuroprotection by freezing ischemic penumbra evolution without cerebral blood flow augmentation with a postsynaptic density-95 protein inhibitor. Stroke. 2011;42(11):3265-70. doi:10.1161/strokeaha.111.618801.
13. Hill MD, Martin RH, Mikulis D, Wong JH, Silver FL, Terbrugge KG et al. Safety and efficacy of NA-1 in patients with iatrogenic stroke after endovascular aneurysm repair (ENACT): a phase 2, randomised, double-blind, placebo-controlled trial. Lancet Neurol. 2012;11(11):942-50. doi:10.1016/s1474-4422(12)70225-9.

14. Sun HS, Doucette TA, Liu Y, Fang Y, Teves L, Aarts M et al. Effectiveness of PSD95 inhibitors in permanent and transient focal ischemia in the rat. Stroke. 2008;39(9):2544-53. doi:10.1161/strokeaha.107.506048.
15. Fisher M, Saver JL. Future directions of acute ischaemic stroke therapy. Lancet Neurol. 2015;14(7):758-67. doi:10.1016/s1474-4422(15)00054-x.
16. Bacigaluppi M, Comi G, Hermann DM. Animal models of ischemic stroke. Part two: modeling cerebral ischemia. Open Neurol J. 2010;4:34-8. doi:10.2174/1874205x01004020034.
17. Jahan R, Stewart D, Vinters HV, Yong W, Vinuela F, Vandeberg P et al. Middle cerebral artery occlusion in the rabbit using selective angiography: application for assessment of thrombolysis. Stroke. 2008;39(5):1613-5. doi:10.1161/STROKEAHA.107.507376.
18. Wey HY, Kroma GM, Li J, Leland MM, Jones L, Duong TQ. MRI of perfusion-diffusion mismatch in non-human primate (baboon) stroke: a preliminary report. Open Neuroimag J. 2011;5:147-52. doi:10.2174/1874440001105010147.
19. Zhang X, Tong F, Li CX, Yan Y, Kempf D, Nair G et al. Temporal evolution of ischemic lesions in nonhuman primates: a diffusion and perfusion MRI study. PLoS One. 2015;10(2):e0117290. doi:10.1371/journal.pone.0117290.
20. Hill NC, Millikan CH, Wakim KG, Sayre GP. Studies in cerebrovascular disease. VII Experimental production of cerebral infarction by intracarotid injection of homologous blood clot: preliminary report. Mayo Clin Proc. 1955;30(26):625-33.
21. Molinari GF. Experimental cerebral infarction. I. Selective segmental occlusion of intracranial arteries in the dog. Stroke. 1970;1(4):224-31.
22. Rink C, Christoforidis G, Abduljalil A, Kontzialis M, Bergdall V, Roy S et al. Minimally invasive neuroradiologic model of preclinical transient middle cerebral artery occlusion in canines. Proc Natl Acad Sci U S A. 2008;105(37):14100-5. doi:10.1073/pnas.0806678105.
23. Purdy PD, Devous MD, Sr., Batjer HH, White CL, 3rd, Meyer Y, Samson DS. Microfibrillar collagen model of canine cerebral infarction. Stroke. 1989;20(10):1361-7.

24. Harris AD, Kosior JC, Ryder RC, Andersen LB, Hu WY, Hudon M et al. MRI of ischemic stroke in canines: applications for monitoring intraarterial thrombolysis. J Magn Reson Imaging. 2007;26(6):1421-8. doi:10.1002/jmri.21189.

25. Shaibani A, Khawar S, Shin W, Cashen TA, Schirf B, Rohany M et al. First results in an MR imaging--compatible canine model of acute stroke. AJNR Am J Neuroradiol. 2006;27(8):1788-93.

26. Ahmed AS, Zellerhoff M, Strother CM, Pulfer KA, Redel T, Deuerling-Zheng Y et al. C-arm CT measurement of cerebral blood volume: an experimental study in canines. AJNR Am J Neuroradiol. 2009;30(5):917-22.

27. van der Bom IMJ, Mehra M, Walvick RP, Chueh J-Y, Gounis MJ. Quantitative evaluation of c-arm CT CBV in a canine model of ischemic stroke. AJNR Am J Neuroradiol. 2011;33:353-8.

28. Brooks OW, King RM, Nossek E, Marosfoi M, Caroff J, Chueh JY et al. A canine model of mechanical thrombectomy in stroke. J Neurointerv Surg. 2019. doi:10.1136/neurintsurg-2019-014969.

29. Anderson WD, Kubicek W. The vertebral-basilar system of dog in relation to man and other mammals. Am J Anat. 1971;132(2):179-88. doi:10.1002/aja.1001320205.

30. Wells AJ, Vink R, Blumbergs PC, Brophy BP, Helps SC, Knox SJ et al. A surgical model of permanent and transient middle cerebral artery stroke in the sheep. PLoS One. 2012;7(7):e42157. doi:10.1371/journal.pone.0042157.

31. Boltze J, Forschler A, Nitzsche B, Waldmin D, Hoffmann A, Boltze CM et al. Permanent middle cerebral artery occlusion in sheep: a novel large animal model of focal cerebral ischemia. J Cereb Blood Flow Metab. 2008;28(12):1951-64. doi:10.1038/jcbfm.2008.89.

32. Platt SR, Holmes SP, Howerth EW, Duberstein KJJ, Dove CR, Kinder HA et al. Development and characterization of a Yucatan miniature biomedical pig permanent middle cerebral artery occlusion stroke model. Exp Transl Stroke Med. 2014;6(1):5. doi:10.1186/2040-7378-6-5.

33. Mehra M, Henninger N, Hirsch JA, Chueh J, Wakhloo AK, Gounis MJ. Preclinical acute ischemic stroke modeling. J Neurointerv Surg. 2012;4(4):307-13. doi:10.1136/neurintsurg-2011-010101.

34. Herrmann AM, Meckel S, Gounis MJ, Kringe L, Motschall E, Mulling C et al. Large animals in neurointerventional research: A systematic review on models, techniques and their application in endovascular procedures for stroke, aneurysms and vascular malformations. J Cereb Blood Flow Metab. 2019;39(3):375-94. doi:10.1177/0271678x19827446.
35. Kang BT, Lee JH, Jung DI, Park C, Gu SH, Jeon HW et al. Canine model of ischemic stroke with permanent middle cerebral artery occlusion: clinical and histopathological findings. J Vet Sci. 2007;8(4):369-76.
36. Harris AD, Kosior RK, Chen HS, Andersen LB, Frayne R. Evolution of hyperacute stroke over 6 hours using serial MR perfusion and diffusion maps. J Magn Reson Imaging. 2009;29(6):1262-70. doi:10.1002/jmri.21763.
37. Christoforidis GA, Vakil P, Ansari SA, Dehkordi FH, Carroll TJ. Impact of Pial Collaterals on Infarct Growth Rate in Experimental Acute Ischemic Stroke. AJNR Am J Neuroradiol. 2017;38(2):270-5. doi:10.3174/ajnr.A5003.
38. Rocha M, Jovin TG. Fast Versus Slow Progressors of Infarct Growth in Large Vessel Occlusion Stroke: Clinical and Research Implications. Stroke. 2017;48(9):2621-7. doi:10.1161/strokeaha.117.017673.
39. Wheeler HM, Mlynash M, Inoue M, Tipirnini A, Liggins J, Bammer R et al. The growth rate of early DWI lesions is highly variable and associated with penumbral salvage and clinical outcomes following endovascular reperfusion. Int J Stroke. 2015;10(5):723-9. doi:10.1111/ijs.12436.
40. Ribo M, Molina CA, Cobo E, Cerda N, Tomasello A, Quesada H et al. Association Between Time to Reperfusion and Outcome Is Primarily Driven by the Time From Imaging to Reperfusion. Stroke. 2016;47(4):999-1004. doi:10.1161/strokeaha.115.011721.
41. Copen WA, Rezai Gharai L, Barak ER, Schwamm LH, Wu O, Kamalian S et al. Existence of the diffusion-perfusion mismatch within 24 hours after onset of acute stroke: dependence on proximal arterial occlusion. Radiology. 2009;250(3):878-86. doi:10.1148/radiol.2503080811.
42. Marchal G, Beaudouin V, Rioux P, de la Sayette V, Le Doze F, Viader F et al. Prolonged persistence of substantial volumes of potentially viable brain tissue after

stroke: a correlative PET-CT study with voxel-based data analysis. Stroke. 1996;27(4):599-606.
43. Schellinger PD, Jansen O, Fiebach JB, Heiland S, Steiner T, Schwab S et al. Monitoring intravenous recombinant tissue plasminogen activator thrombolysis for acute ischemic stroke with diffusion and perfusion MRI. Stroke. 2000;31(6):1318-28.
44. Wu O, Koroshetz WJ, Ostergaard L, Buonanno FS, Copen WA, Gonzalez RG et al. Predicting tissue outcome in acute human cerebral ischemia using combined diffusion- and perfusion-weighted MR imaging. Stroke. 2001;32(4):933-42.
45. Ostergaard L, Sorensen AG, Chesler DA, Weisskoff RM, Koroshetz WJ, Wu O et al. Combined diffusion-weighted and perfusion-weighted flow heterogeneity magnetic resonance imaging in acute stroke. Stroke. 2000;31(5):1097-103.
46. Schaefer PW, Hunter GJ, He J, Hamberg LM, Sorensen AG, Schwamm LH et al. Predicting cerebral ischemic infarct volume with diffusion and perfusion MR imaging. AJNR Am J Neuroradiol. 2002;23(10):1785-94.
47. Wheeler HM, Mlynash M, Inoue M, Tipirneni A, Liggins J, Zaharchuk G et al. Early diffusion-weighted imaging and perfusion-weighted imaging lesion volumes forecast final infarct size in DEFUSE 2. Stroke. 2013;44(3):681-5. doi:10.1161/strokeaha.111.000135.
48. Olivot JM, Mlynash M, Thijs VN, Purushotham A, Kemp S, Lansberg MG et al. Geography, structure, and evolution of diffusion and perfusion lesions in Diffusion and perfusion imaging Evaluation For Understanding Stroke Evolution (DEFUSE). Stroke. 2009;40(10):3245-51. doi:10.1161/strokeaha.109.558635.
49. Rordorf G, Koroshetz WJ, Copen WA, Cramer SC, Schaefer PW, Budzik RF, Jr. et al. Regional ischemia and ischemic injury in patients with acute middle cerebral artery stroke as defined by early diffusion-weighted and perfusion-weighted MRI. Stroke. 1998;29(5):939-43.
50. Le Bihan D, Breton E, Lallemand D, Grenier P, Cabanis E, Laval-Jeantet M. MR imaging of intravoxel incoherent motions: application to diffusion and perfusion in neurologic disorders. Radiology. 1986;161(2):401-7. doi:10.1148/radiology.161.2.3763909.

51. Wesbey GE, Moseley ME, Ehman RL. Translational molecular self-diffusion in magnetic resonance imaging. II. Measurement of the self-diffusion coefficient. Invest Radiol. 1984;19(6):491-8.
52. Moseley ME, Cohen Y, Mintorovitch J, Chileuitt L, Shimizu H, Kucharczyk J et al. Early detection of regional cerebral ischemia in cats: comparison of diffusion- and T2-weighted MRI and spectroscopy. Magn Reson Med. 1990;14(2):330-46.
53. Copen WA, Schaefer PW, Wu O. MR perfusion imaging in acute ischemic stroke. Neuroimaging Clin N Am. 2011;21(2):259-83. doi:10.1016/j.nic.2011.02.007.
54. Neumann-Haefelin T, Wittsack HJ, Wenserski F, Siebler M, Seitz RJ, Modder U et al. Diffusion- and perfusion-weighted MRI. The DWI/PWI mismatch region in acute stroke. Stroke. 1999;30(8):1591-7.
55. Albers GW. Expanding the window for thrombolytic therapy in acute stroke. The potential role of acute MRI for patient selection. Stroke. 1999;30(10):2230-7.
56. Rivers CS, Wardlaw JM, Armitage PA, Bastin ME, Carpenter TK, Cvoro V et al. Do acute diffusion- and perfusion-weighted MRI lesions identify final infarct volume in ischemic stroke? Stroke. 2006;37(1):98-104. doi:10.1161/01.STR.0000195197.66606.bb.
57. Takasawa M, Jones PS, Guadagno JV, Christensen S, Fryer TD, Harding S et al. How reliable is perfusion MR in acute stroke? Validation and determination of the penumbra threshold against quantitative PET. Stroke. 2008;39(3):870-7. doi:10.1161/strokeaha.107.500090.
58. Baird AE, Lovblad KO, Dashe JF, Connor A, Burzynski C, Schlaug G et al. Clinical correlations of diffusion and perfusion lesion volumes in acute ischemic stroke. Cerebrovasc Dis. 2000;10(6):441-8. doi:10.1159/000016105.
59. Barber PA, Parsons MW, Desmond PM, Bennett DA, Donnan GA, Tress BM et al. The use of PWI and DWI measures in the design of "proof-of-concept" stroke trials. J Neuroimaging. 2004;14(2):123-32.
60. Butcher K, Parsons M, Baird T, Barber A, Donnan G, Desmond P et al. Perfusion thresholds in acute stroke thrombolysis. Stroke. 2003;34(9):2159-64. doi:10.1161/01.str.0000086529.83878.a2.

61. Parsons MW, Barber PA, Chalk J, Darby DG, Rose S, Desmond PM et al. Diffusion- and perfusion-weighted MRI response to thrombolysis in stroke. Ann Neurol. 2002;51(1):28-37.
62. Parsons MW, Yang Q, Barber PA, Darby DG, Desmond PM, Gerraty RP et al. Perfusion magnetic resonance imaging maps in hyperacute stroke: relative cerebral blood flow most accurately identifies tissue destined to infarct. Stroke. 2001;32(7):1581-7.
63. Rohl L, Geday J, Ostergaard L, Simonsen CZ, Vestergaard-Poulsen P, Andersen G et al. Correlation between diffusion- and perfusion-weighted MRI and neurological deficit measured by the Scandinavian Stroke Scale and Barthel Index in hyperacute subcortical stroke (< or = 6 hours). Cerebrovasc Dis. 2001;12(3):203-13. doi:10.1159/000047705.
64. Rohl L, Ostergaard L, Simonsen CZ, Vestergaard-Poulsen P, Andersen G, Sakoh M et al. Viability thresholds of ischemic penumbra of hyperacute stroke defined by perfusion-weighted MRI and apparent diffusion coefficient. Stroke. 2001;32(5):1140-6.
65. Rose SE, Chalk JB, Griffin MP, Janke AL, Chen F, McLachan GJ et al. MRI based diffusion and perfusion predictive model to estimate stroke evolution. Magn Reson Imaging. 2001;19(8):1043-53.
66. Rose SE, Janke AL, Griffin M, Finnigan S, Chalk JB. Improved prediction of final infarct volume using bolus delay-corrected perfusion-weighted MRI: implications for the ischemic penumbra. Stroke. 2004;35(11):2466-71. doi:10.1161/01.STR.0000145199.64907.5a.
67. Ueda T, Yuh WT, Maley JE, Quets JP, Hahn PY, Magnotta VA. Outcome of acute ischemic lesions evaluated by diffusion and perfusion MR imaging. AJNR Am J Neuroradiol. 1999;20(6):983-9.
68. Yoo AJ, Verduzco LA, Schaefer PW, Hirsch JA, Rabinov JD, Gonzalez RG. MRI-based selection for intra-arterial stroke therapy: value of pretreatment diffusion-weighted imaging lesion volume in selecting patients with acute stroke who will benefit from early recanalization. Stroke. 2009;40(6):2046-54. doi:10.1161/strokeaha.108.541656.
69. Mlynash M, Lansberg MG, De Silva DA, Lee J, Christensen S, Straka M et al. Refining the definition of the malignant profile: insights from the DEFUSE-EPITHET pooled data set. Stroke. 2011;42(5):1270-5. doi:10.1161/strokeaha.110.601609.

70. Kakuda W, Lansberg MG, Thijs VN, Kemp SM, Bammer R, Wechsler LR et al. Optimal definition for PWI/DWI mismatch in acute ischemic stroke patients. J Cereb Blood Flow Metab. 2008;28(5):887-91. doi:10.1038/sj.jcbfm.9600604.
71. Kim S, Kang M, Choi S, Kim DW. Mismatch of delayed perfusion volume between TTP and Tmax map of perfusion MRI. Clin Imaging. 2016;40(1):63-7. doi:10.1016/j.clinimag.2015.10.005.
72. Thomalla GJ, Kucinski T, Schoder V, Fiehler J, Knab R, Zeumer H et al. Prediction of malignant middle cerebral artery infarction by early perfusion- and diffusion-weighted magnetic resonance imaging. Stroke. 2003;34(8):1892-9. doi:10.1161/01.str.0000081985.44625.b6.
73. Wouters A, Christensen S, Straka M, Mlynash M, Liggins J, Bammer R et al. A Comparison of Relative Time to Peak and Tmax for Mismatch-Based Patient Selection. Front Neurol. 2017;8:539. doi:10.3389/fneur.2017.00539.
74. Zaro-Weber O, Moeller-Hartmann W, Siegmund D, Kandziora A, Schuster A, Heiss WD et al. MRI-based mismatch detection in acute ischemic stroke: Optimal PWI maps and thresholds validated with PET. J Cereb Blood Flow Metab. 2017;37(9):3176-83. doi:10.1177/0271678x16685574.
75. Sobesky J, Zaro Weber O, Lehnhardt FG, Hesselmann V, Thiel A, Dohmen C et al. Which time-to-peak threshold best identifies penumbral flow? A comparison of perfusion-weighted magnetic resonance imaging and positron emission tomography in acute ischemic stroke. Stroke. 2004;35(12):2843-7. doi:10.1161/01.STR.0000147043.29399.f6.
76. Reimer J, Montag C, Schuster A, Moeller-Hartmann W, Sobesky J, Heiss WD et al. Is Perfusion MRI without Deconvolution Reliable for Mismatch Detection in Acute Stroke? Validation with 15O-Positron Emission Tomography. Cerebrovasc Dis. 2018;46(1-2):16-23. doi:10.1159/000490424.
77. Ogata T, Nagakane Y, Christensen S, Ma H, Campbell BC, Churilov L et al. A topographic study of the evolution of the MR DWI/PWI mismatch pattern and its clinical impact: a study by the EPITHET and DEFUSE Investigators. Stroke. 2011;42(6):1596-601. doi:10.1161/strokeaha.110.609016.

78. Lansberg MG, Straka M, Kemp S, Mlynash M, Wechsler LR, Jovin TG et al. MRI profile and response to endovascular reperfusion after stroke (DEFUSE 2): a prospective cohort study. Lancet Neurol. 2012;11(10):860-7. doi:10.1016/s1474-4422(12)70203-x.
79. Short CE. Principles & Practice of Veterinary Anesthesia. Williams & Wilkins; 1987.
80. Bratane BT, Bastan B, Fisher M, Bouley J, Henninger N. Ischemic lesion volume determination on diffusion weighted images vs. apparent diffusion coefficient maps. Brain Res. 2009;1279:182-8. doi:10.1016/j.brainres.2009.05.002.
81. Kang BT, Jang DP, Gu SH, Lee JH, Jung DI, Lim CY et al. MRI features in a canine model of ischemic stroke: correlation between lesion volume and neurobehavioral status during the subacute stage. Comp Med. 2009;59(5):459-64.
82. Faul F, Erdfelder E, Lang AG, Buchner A. G*Power 3: a flexible statistical power analysis program for the social, behavioral, and biomedical sciences. Behav Res Methods. 2007;39(2):175-91.
83. Jahng GH, Li KL, Ostergaard L, Calamante F. Perfusion magnetic resonance imaging: a comprehensive update on principles and techniques. Korean J Radiol. 2014;15(5):554-77. doi:10.3348/kjr.2014.15.5.554.
84. Calamante F, Thomas DL, Pell GS, Wiersma J, Turner R. Measuring cerebral blood flow using magnetic resonance imaging techniques. J Cereb Blood Flow Metab. 1999;19(7):701-35. doi:10.1097/00004647-199907000-00001.
85. Perthen JE, Calamante F, Gadian DG, Connelly A. Is quantification of bolus tracking MRI reliable without deconvolution? Magn Reson Med. 2002;47(1):61-7.
86. Christensen S, Mouridsen K, Wu O, Hjort N, Karstoft H, Thomalla G et al. Comparison of 10 perfusion MRI parameters in 97 sub-6-hour stroke patients using voxel-based receiver operating characteristics analysis. Stroke. 2009;40(6):2055-61. doi:10.1161/strokeaha.108.546069.
87. Calamante F. Arterial input function in perfusion MRI: a comprehensive review. Prog Nucl Magn Reson Spectrosc. 2013;74:1-32. doi:10.1016/j.pnmrs.2013.04.002.
88. Motta M, Ramadan A, Hillis AE, Gottesman RF, Leigh R. Diffusion-perfusion mismatch: an opportunity for improvement in cortical function. Front Neurol. 2014;5:280. doi:10.3389/fneur.2014.00280.

89. Wittsack HJ, Ritzl A, Fink GR, Wenserski F, Siebler M, Seitz RJ et al. MR imaging in acute stroke: diffusion-weighted and perfusion imaging parameters for predicting infarct size. Radiology. 2002;222(2):397-403. doi:10.1148/radiol.2222001731.
90. Grandin CB, Duprez TP, Smith AM, Oppenheim C, Peeters A, Robert AR et al. Which MR-derived perfusion parameters are the best predictors of infarct growth in hyperacute stroke? Comparative study between relative and quantitative measurements. Radiology. 2002;223(2):361-70. doi:10.1148/radiol.2232010673.
91. Drier A, Tourdias T, Attal Y, Sibon I, Mutlu G, Lehericy S et al. Prediction of subacute infarct size in acute middle cerebral artery stroke: comparison of perfusion-weighted imaging and apparent diffusion coefficient maps. Radiology. 2012;265(2):511-7. doi:10.1148/radiol.12112430.
92. Zaro-Weber O, Moeller-Hartmann W, Heiss WD, Sobesky J. MRI perfusion maps in acute stroke validated with 15O-water positron emission tomography. Stroke. 2010;41(3):443-9. doi:10.1161/strokeaha.109.569889.
93. Werner P, Saur D, Zeisig V, Ettrich B, Patt M, Sattler B et al. Simultaneous PET/MRI in stroke: a case series. J Cereb Blood Flow Metab. 2015;35(9):1421-5. doi:10.1038/jcbfm.2015.158.
94. Martel AL, Allder SJ, Delay GS, Morgan PS, Moody AA. Perfusion MRI of infarcted and noninfarcted brain tissue in stroke: a comparison of conventional hemodynamic imaging and factor analysis of dynamic studies. Invest Radiol. 2001;36(7):378-85.
95. Hartmann A, Driesen A, Lautenschlager IE, Scholz VB, Schmidt MJ. Quantitative analysis of brain perfusion in healthy dogs by means of magnetic resonance imaging. Am J Vet Res. 2016;77(11):1227-35. doi:10.2460/ajvr.77.11.1227.
96. Meijs M, Christensen S, Lansberg MG, Albers GW, Calamante F. Analysis of perfusion MRI in stroke: To deconvolve, or not to deconvolve. Magn Reson Med. 2016;76(4):1282-90. doi:10.1002/mrm.26024.

Figure Legends

Fig. 1 Placement of an autologous clot in the middle cerebral artery (MCA) of the dog. (**a**) Digital Subtraction Angiography (DSA) prior to clot placement is shown. The arrows indicate the location of the MCA (**b**) Total MCA occlusion is shown in DSA post-clot placement. The dashed arrows depict the original course of the MCA, which is now absent. (**c**) Time-of-flight (ToF) MRI shows an open internal carotid artery (ICA) and an occluded MCA.

Fig. 2 Flowchart of image analysis. Apparent diffusion coefficient (ADC) and time-to-peak (TTP) maps were generated from diffusion-weighted imaging (DWI) and perfusion-weighted imaging (PWI), respectively. ADC maps were used to calculate the final infarct volume. The entire brain in TTP maps was normalized with respect to a representative area on the contralateral side of the infarct region to generate relative TTP (rTTP) maps. rTTP maps were registered with ADC maps to count the voxels within the infarct volume. All voxels within the ADC-defined lesion were binned into one of four categories in the rTTP map. The total size of each bin, across the entire lesion volume, was used to predict the rate of infarct evolution.

Fig. 3 Representative animal from the fast evolver group (Animal #4 from Table 1). (**a**) Final diffusion-weighted imaging (DWI) image showing the total extent of the infarct as a hyperintense region. (**b**) Apparent diffusion coefficient (ADC) map showing a hypointense region indicating the extent of infarct. The red line on the scale bar indicates the intensity

level of the infarct region. (**c**) Post-mortem triphenyltetrazolium chloride (TTC) staining showing the final histological infarct size. Scale bar: 10 mm. (**d**) Relative time-to-peak (rTTP) map derived from perfusion-weighted imaging (PWI) images. The color intensity of the infarct area voxels indicate an elevated intensity at or above the 20-s delay. Digital Subtraction Angiography (DSA) is shown in early (**e**) and delayed phase (**f**), which denote a lack of collaterals in the right hemisphere. The arrows indicate the location of the clot.

Fig. 4 Representative animal from the slow evolver group (Animal #1 from Table 1). (**a**) Final diffusion-weighted imaging (DWI) image showing the total extent of the infarct as a hyperintense region. (**b**) Apparent diffusion coefficient (ADC) map showing a hypointense region indicating the extent of infarct. The red line on the scale bar indicates the intensity level of the infarct region. (**c**) Post-mortem triphenyltetrazolium chloride (TTC) staining showing the final histological infarct size. Scale bar: 10 mm. (**d**) Relative time-to-peak (rTTP) map derived from perfusion-weighted imaging (PWI) images. The area of occlusion is seen only slightly elevated with a few voxels above the 20-s delay. Digital Subtraction Angiography (DSA) is shown in early (**e**) and delayed phase (**f**), which highlights the impact of the collaterals in the left hemisphere. The arrows indicate the location of the clot.

Fig. 5 Quantification of fast and slow evolvers using diffusion-weighted imaging (DWI) apparent diffusion coefficient (ADC) maps and perfusion-weighted imaging (PWI) time-to-peak (TTP) maps. (**a**) Ischemic core evolution as derived by ADC-thresholded maps and dichotomized to fast (orange) versus slow (blue) evolvers are shown. Based on lesion

growth rate, animals were divided into fast (>50% total volume within 2 h) and slow (<50% total volume within 2 h) evolver groups. The plot shows the progression of slow and fast evolvers with the greatest difference occurring at about 2 h. Individual growth curves are shown for each animal in lighter shade. Error bars indicate SEM. (**b**) Correlation plot is shown indicating the agreement of infarct volumes between the final DWI image and the TTP map generated from the initial PWI images (R^2 = 0.99). The dotted lines indicate 95% confidence level. (**c**) Histogram binning from rTTP maps for fast and slow evolvers are shown. The voxels in the “slight delay” bin (4−8 s) of fast evolvers are significantly fewer compared to that of slow evolvers (**p < 0.0001). The dashed line near the left axis of the plot shows a cutoff at ~34%, which distinguishes between the fast and slow evolvers in the “slight delay” bin. The voxels in the “extended delay” bin (19+ s) of fast evolvers are significantly more compared to that of slow evolvers (*p = 0.0013). The dashed line near the right axis of the plot shows a cutoff at ~42%, which distinguishes between the fast and slow evolvers in the “extended delay” bin. The two middle bins of “moderate delay” (9−13 s) and “long delay” (14−18 s) did not show any significant differences between the slow and fast evolvers. Error bars indicate SEM.

Title:

Infarct Evolution in a Large Animal Model of Middle Cerebral Artery Occlusion

Authors:

*Mohammed Salman Shazeeb[1,2] (Corresponding author)
*Robert M. King[1,3]
Olivia W. Brooks[1,4]
Ajit S. Puri[1]
Nils Henninger[5,6]
Johannes Boltze[7]
Matthew J. Gounis[1,2]

[1]New England Center for Stroke Research, Department of Radiology
University of Massachusetts Medical School, Worcester, MA, 01655, USA.

[2]Image Processing and Analysis Core, Department of Radiology
University of Massachusetts Medical School, Worcester, MA, 01655, USA.

[3]Department of Biomedical Engineering
Worcester Polytechnic Institute, Worcester, MA, 01609, USA.

[4]St. George's University School of Medicine, Grenada, West Indies

Departments of [5]Neurology and [6]Psychiatry
University of Massachusetts Medical School, Worcester, MA, 01655, USA.

[7]University of Warwick, School of Life Sciences, Coventry, CV4 7AL, United Kingdom

*These authors contributed equally to this work

Corresponding address:

Mohammed Salman Shazeeb, Ph.D.
Department of Radiology
Division of Biomedical Imaging and Bioengineering
University of Massachusetts Medical School
55 Lake Avenue North, S7-410, Worcester, MA 01655, USA
E-mail: Mohammed.Shazeeb@umassmed.edu
Phone: 508-856-4255
Fax: 508-856-6363

Sources of funding: Dr. Henninger is supported by K08NS091499 from the National Institute of Neurological Disorders and Stroke (NINDS) of the National Institutes of Health (NIH). The content is solely the responsibility of the authors and does not necessarily represent the official views of the NIH. Dr. Gounis has received research support from the NIH, the United States – Israel Binational Science Foundation, Anaconda, Cerenovus, Ceretrieve, Cook Medical, Gentuity, Imperative Care, InNeuroCo, Magneto, Microvention, Medtronic Neurovascular, MIVI Neurosciences, Neuravi, Neurogami, Philips Healthcare, Rapid Medical, Route 92 Medical, Stryker Neurovascular, Syntheon, and the Wyss Institute.

Running headline: Infarct Evolution in a Canine Stroke Model

Abstract

Mechanical thrombectomy for the treatment of ischemic stroke shows high rates of recanalization; however, some patients still have a poor clinical outcome. A proposed reason for this relates to the fact that the ischemic infarct growth differs significantly between patients. While some patients demonstrate rapid evolution of their infarct core (fast evolvers), others have substantial potentially salvageable penumbral tissue even hours after initial vessel occlusion (slow evolvers). We show that the dog middle cerebral artery occlusion model recapitulates this key aspect of human stroke rendering it a highly desirable model to develop novel multimodal treatments to improve clinical outcomes. Moreover, this model is well suited to develop novel image analysis techniques that allow for improved lesion evolution prediction; we provide proof-of-concept that MRI perfusion-based time-to-peak maps can be utilized to predict the rate of infarct growth as validated by apparent diffusion coefficient derived lesion maps allowing reliable classification of

dogs into fast versus slow evolvers enabling more robust study design for interventional research.

Key words: dog, middle cerebral artery occlusion, infarct growth rate, perfusion MRI, time-to-peak, stroke.

Introduction

In recent years, randomized-controlled trials have shown that mechanical thrombectomy is a highly effective treatment for selected ischemic stroke patients with emergent large vessel occlusion (ELVO) [1-3]. Although clinical trials and uncontrolled stroke registries report successful recanalization of the primary artery in approximately 85% [4, 5], rates of good clinical outcomes have not yet matched the high rate of technical success. For this reason, novel approaches to multimodal intervention that includes neuroprotection, adjunctive technology to augment brain perfusion, thrombolysis, and recanalization with thrombectomy promise to maximize the probability of a good clinical outcome after ELVO. In particular, methods that can slow infarct progression may expand the availability of mechanical thrombectomy for ELVO patients that present beyond established treatment windows [6, 7]. Approaches under development include transient aortic occlusion [8], stimulation of circle of Willis nerve fibers [9], mild induced hypertension [10], and inhalation of nitric oxide [11]. Perhaps the greatest opportunity is re-exploration of pharmacological neuroprotection combined with mechanical thrombectomy [12-15].

Although multiple animal stroke models are available in a variety of species to study stroke pathophysiology and possible treatment modalities [16], only larger animal species such as rabbits [17], non-human primates [18, 19], and dogs [20-27] are suitable for creating ELVO via an endovascular approach without performing a craniotomy. However, to date only the dog model allows simulation of mechanical thrombectomy for ELVO [28]. Moreover, the gyrencephalic brain of dogs renders it structurally and functionally more similar to the human brain than that of rodents [29]. Unlike sheep [30,

31] and swine [32], dogs do not possess a *rete mirabile*, thus allowing direct endovascular access to the middle cerebral artery (MCA) for creating an occlusion as well as achieving mechanical recanalization [28, 33, 34]. The dog ELVO model has been developed to allow for the assessment of neuroprotectants and other novel therapeutics [35]. Prior studies suggested that the dog model may be limited by its variable ischemic lesion evolution possibly due to irregular collateral circulation [36, 37]. Here we formally explored the possibility that this variability is similar to the human condition and contributes to the different rates of ~~stroke~~infarct evolution [38]: 1.) fast progressors, who experience rapid infarct growth with a large ischemic core and failing collaterals despite an early diagnosis within 6 h of stroke onset [39, 40]; and 2) slow progressors, who experience slow infarct growth maintaining a small ischemic core and good collaterals with significant salvageable tissue beyond the 6 h time window [41, 42].

Diffusion- (DWI) and perfusion-weighted imaging (PWI) are common magnetic resonance imaging (MRI) techniques used for diagnosing ischemic stroke in the clinical setting [43-49]. The DWI-derived apparent diffusion coefficient (ADC) of cerebral tissue decreases within the region of the irreversibly injured infarct core that can be detected using appropriate thresholds [50-52]. Several PWI parameters derived from dynamic susceptibility contrast (DSC)-MRI including cerebral blood flow (CBF), cerebral blood volume (CBV), mean transit time (MTT), time of maximum value of the tissue residue function (Tmax), bolus arrival time (BAT), and time-to-peak (TTP) concentration become altered as normal cerebral tissue progresses from ischemia to infarction [53]. The DWI/PWI mismatch has been used to predict the extent of infarction and identify patients likely to benefit from reperfusion therapy [54, 55]. However, depending on the PWI

parameter used and the method implemented to compute it, studies have reported an inconsistency in the identification of the final infarct volume especially when using parameters like CBF and MTT [53, 56-68]. On the other hand, PWI parameters like Tmax and TTP have been shown to more accurately estimate the final infarct size [54, 69-77].

The DEFUSE 2 clinical trials reliably showed that patients with target mismatch (based on Tmax thresholds) who underwent early reperfusion after endovascular stroke treatment had more favorable clinical outcomes compared to patients without target mismatch [78]. In a previous dog ELVO model an infarct growth model was developed to predict the infarct growth rate and final infarct volume based on DWI lesion volume and pial collateral quantification from computed tomography (CT) angiograms [37]. However, this model was based on fast evolvers and thus it is uncertain whether results can be translated to slow evolvers. The ability to differentiate fast from slow evolvers early on is an important issue to minimize bias in studies utilizing the dog model to assess novel treatment approaches. To address this issue, we leveraged the presence of slow versus fast evolving ischemic lesions in our established dog ELVO model to predict the infarct evolution using PWI-based TTP maps, derived from DSC-MRI, based only on the first PWI image acquired after the onset of stroke. Correct classification of the infarct evolution from study inception has the advantage to exclude one type of progressor or to prospectively enter animals into appropriate cohorts in therapeutic studies, thereby increasing the scientific rigor.

Materials and Methods

Animal preparation

All animal research procedures were performed as approved by the Institutional Animal Care and Use Committee (IACUC) of the University of Massachusetts Medical School (Worcester, MA, USA). Fourteen purpose-bred dogs (8 females and 6 males; weight: 8.2–23.9 kg; age: 6.5–36 months) were used in this study. Details of the subject demographics are provided in Table 1. On the day of surgery, the animals were sedated and pre-treated with a single dose of intramuscular acepromazine (0.06 mg/kg), buprenorphine (0.02 mg/kg), and glycopyrrolate (0.01 mg/kg). Anesthesia was induced with an intravenous dose of propofol (3–4 mg/kg), and the animal was intubated. Anesthesia was maintained by mechanical ventilation with 1–3% isoflurane in air. Throughout anesthesia, animals were monitored by electrocardiogram (ECG), peripheral capillary oxygen saturation (spO_2), invasive or non-invasive arterial blood pressure, rectal temperature, and end-tidal CO_2. All vital measurements were maintained within the physiological range [79]. Using a modified Seldinger technique, an 8F hemostatic introducer was placed in the right femoral artery to allow endovascular access and blood draw for preparing blood clots as previously described in detail [28]. A 6-french Navien-072 catheter (Medtronic Neurovascular, Irvine, CA) was navigated under fluoroscopic guidance to the origin of the right or left internal carotid artery (ICA), at which point an autologous clot [28] was injected and advanced to permanently occlude the MCA (Fig. 1). The side of clot injection was selected on the basis of the larger diameter and length of non-tortuous cervical ICA for delivery of this relatively large catheter.

Imaging protocol

Once correct clot placement at the origin of the MCA was confirmed by fluoroscopy (Allura Xper FD20; Philips Healthcare, Best, the Netherlands), the animal was transferred

to the MRI scanner (Phillips Achieva/Phillips Ingenia 3T, Philips Healthcare), which is physically adjacent to the angiography suite. An 8-channel knee coil (Philips Healthcare) was used to acquire the brain scans. The imaging protocol included time-of-flight (ToF) imaging (TR/TE 20/4 ms, FA = 20^{o}, matrix 332 × 212), DWI (TR/TE 2600/76 ms, FA = 90^{o}, b-value = 0, 1000 s/mm^{2}, NSA = 6, matrix 144 × 144), PWI (TR/TE 1500/20.1 ms, FA = 40^{o}, 60 dynamics, matrix 320 × 320), and T2-weighted (T2W)-FLAIR imaging (TR/TE 11000/125 ms, TI 2800 ms, FA = 90^{o}, ETL = 27, matrix = 288 × 288). FLAIR imaging was used to rule out the possibility of subarachnoid hemorrhage. For PWI, 0.2 mmol/kg of gadopentetate dimeglumine (Magnevist, Bayer Healthcare Pharmaceuticals, Leverkusen, Germany) was injected intravenously (IV) after the second of 60 dynamic scans (total scan time = 90 s), followed by 15 ml saline bolus. DWI was obtained approximately every half hour up to 4.5 h post-clot injection. To calculate the infarct core volume, ADC maps were generated from the DWI images. Once the final diffusion image was acquired, the animal was euthanized, and in selected cases the brain was harvested immediately for histological assessment to confirm the final infarct size.

Image analysis

In order to assess the rate of ~~stroke~~infarct evolution based on DWI images, ADC maps were generated using MATLAB (The Mathworks, Inc., Natick, MA) and the datasets were binned in aggregates of 30 min. Since the goal of the study was to assess the rate of infarct evolution rather than the overall size of the infarct, the infarct size at each time-point was normalized by the final volume. When DWI was unavailable at a time point, linear interpolation was used to estimate the size of the normalized infarct.

Calculation of TTP maps was done offline using ImageJ (Rasband W. ImageJ. Bethesda, MD: http://rsb.info.nih.gov/ij/; 1997–2006) and MATLAB. The dynamic scans from PWI were used to segment the entire brain region in ImageJ. Scripts were written in MATLAB to calculate the TTP maps using the segmented brain slices from the dynamic scans on a ~~pixel~~voxel-by-~~pixel~~voxel basis by locating the dynamic scan that contained the minimum intensity value. ~~The~~To obtain a relative TTP (rTTP) map, TTP maps were ~~then~~ normalized by ~~subtraction of a~~ subtracting the mean TTP derived from a contralateral region of interest (ROI~~)~~; positioned in the periventricular area of the unaffected hemisphere in the mid-brain region) from the absolute TTP in each ~~pixel, yielding a relative TTP (rTTP) map~~voxel using the following equation:

$$rTTP_{map} = TTP_{map} - \frac{1}{n}\sum_{i=1}^{n}(ROI_{contralateral})_i$$

where *n* is the total number of voxels in the contralateral ROI.

To allow for exact voxel-wise analysis, all brain slices from the respective ADC and TTP maps were co-registered prior to analysis. This was accomplished by registering the B0 images from the DWI acquisition to the raw PWI images using a Dice similarity coefficient to confirm the best possible registration. This affine transformation was then applied to the ADC maps, which registered them to the rTTP maps. The areas defined as infarct on the final DWI were used to isolate only the voxels within the rTTP maps that ultimately evolved to infarction. The voxels on the rTTP maps were categorized into 4 bins: 4–8 s (slight delay), 9–13 s (moderate delay), 14–18 s (long delay), and 19+ s (extended delay). This categorization was used to predict the rate of ~~stroke~~infarct evolution using the rTTP maps and comparing them to the true rate of ~~stroke~~infarct

evolution as measured using serial DWI. A summary of the image analysis is shown in Fig. 2. An rTTP ~~stroke rate~~infarct evolution (rTTPIE) index ~~(rTTP-SRI)~~ was also calculated using the ratio of the rTTP map voxels in the extended delay and slight delay bins to quantify the rate of ~~stroke~~infarct evolution in fast and slow evolvers (Table 1). An ~~rTTP-SRI~~rTTPIE index greater than 1 would indicate a fast evolver and less than 1 would indicate a slow evolver.

Final infarct determination

To minimize confounding of MRI to histology-determined infarct size, we used the ADC-thresholded core assessed on the final image set to determine final infarct volume, which has been previously shown to have a high correlation with TTC-based histology [80, 81]. In addition, we used a subset of animals to assess the final infarct volume histologically. Following extraction, brains were placed in a -80°C freezer for approximately 20 min and then cut into approximately 5-mm thick sections. Each section was stained with 2,3,5-triphenyltetrazolium (TTC) for final infarct volume assessment.

Statistical analysis

All statistical analyses were done in R (R Development Core Team (2018). R: A Language and Environment for Statistical Computing (Version 3.5.2) [Software]. Vienna, Austria: R Foundation for Statistical Computing. Retrieved from http://www.R-project.org). For demographic data, analysis of variance (ANOVA) was used to identify any differences between the slow and fast evolvers. The Pearson product–moment correlation coefficient was used to check for significance of the correlations between the infarct volumes of the DWI and PWI images. For the comparison between histograms of the two groups (slow

and fast evolvers), a paired t-test was used. Fisher's exact test was used to examine the significance of association between the rTTP map and DWI categorization of fast and slow evolvers, i.e. to identify the capability of the rTTP maps to predict the DWI results. A two-sided $p < 0.05$ was considered significant in all analyses. A *post-hoc* power analysis was also performed using $\alpha = 0.05$ to verify the statistical power of the significant differences between the fast and slow evolvers in this study using the G*Power software package [82].

Results

MCA occlusion

Embolic MCA occlusion was successfully induced in all animals (n = 14) as confirmed by digital subtraction angiography (Fig. 1a, b). The persistence of the MCA occlusion was confirmed by ToF-MRI (Fig. 1c) in each animal. None of the animals displayed any hemorrhagic transformation (data not shown).

Imaging characteristics of fast evolvers

Figure 3 depicts a representative animal (Animal #4 from Table 1) that was assigned to the fast evolver group (based on the DWI designation discussed below). A single coronal slice is shown indicating an area of restricted diffusion in the right MCA territory (Fig. 3a). The corresponding ADC map of the same slice shows a hypointense region indicating the extent of infarct with a lesion averaged ADC value of ~0.5×10^{-3} mm^2/s (Fig. 3b). The corresponding TTC-stained brain section shows concordance of the histology with the ADC-defined region of infarction (Fig. 3c). The rTTP map,

corresponding to the ADC map, derived from PWI images is displayed using a pseudo-color map indicating the same infarct region (Fig. 3d). The color intensity of the voxels indicates that the infarct area with an elevated intensity are at or above ~20 s. Images from DSA in the early (Fig. 3e) and delayed (Fig. 3f) phase indicate a lack of collaterals in the right hemisphere.

Imaging characteristics of slow evolvers

Figure 4 shows a representative animal (Animal #1 from Table 1) that was assigned to the slow evolver group (based on the DWI designation discussed below), which revealed a smaller lesion size compared to the fast evolver in Fig. 3. A single coronal slice is shown where the infarct region is visible as an area of restricted diffusion in the left hemisphere (Fig. 4a). The corresponding ADC map of the same slice shows a hypointense region indicating the extent of infarct with an ADC value of ~0.5 × 10^{-3} mm^2/s (Fig. 4b). The corresponding TTC-stained brain section confirms the ADC-defined region of infarct (Fig. 4c). The TTP map, corresponding to the slice from the ADC map, derived from PWI images is displayed using a pseudo-color map indicating the same infarct region (Fig. 4d). The color intensity of the voxels in the infarct area only have a slightly elevated intensity with only a few voxels above ~20 s, which is in contrast to the elevated intensities observed in the fast evolver (Fig. 3d). Images from DSA in the early (Fig. 4e) and delayed (Fig. 4f) phase highlight the impact of the collaterals in the left hemisphere.

Fast and slow evolver designation using DWI

Based on the normalized ~~stroke~~infarct volume as a function of time using DWI (Fig. 5a), animals were categorized to fast versus slow evolvers. After MCA occlusion, fast

evolvers showed a constant growth in the ADC-thresholded infarct volume during the first 2 h at which point infarct growth plateaued to reach the final infarct size. Slow evolvers demonstrated a relatively slow infarct core evolution in the first 2 h with a secondary more rapid constant growth occurring afterwards until the final infarct size was reached at approximately 4 h after MCA occlusion. Thus, animals displaying more than 50% of total infarct volume within 2 h were assigned to the fast evolver group and animals displaying less than 50% of the total infarct volume within 2 h were assigned to the slow evolver group. Based on this definition, each animal in this study was designated with an infarct evolution rate (Table 1). A comparison between the demographics (sex, age, and weight) of the fast and slow evolvers did not show any significant difference (Table 2). The vital measurements between the groups also did not show any significant difference (data not shown)

Prediction of fast versus slow evolvers using initial PWI

The correlation plot (Fig. 5b) shows the agreement of the infarct volumes between the final DWI image and the TTP map generated from the initial PWI images ($R^2 = 0.99$). Based on the relative number of voxels within the "slight delay" and "extended delay" categories, animals were classified into fast and slow evolvers (Fig. 5c): the respective cutoff marks to distinguish between slow and fast evolvers were ~34% for the "slight delay" and ~42% for the "extended delay" bins~~.~~ based on the minimal distance (halfway point) between the boundary points of each category. This classification was more apparent using the ~~rTTP-SRI~~rTTPIE index, which demonstrated a significant difference between the fast and slow evolvers (Table 2). For the remaining bins, the fast and slow evolvers did not show a significant difference. This rTTP-based classification correctly

predicted the DWI results of all fourteen animals ($p < 0.01$, Fishers exact test for classification). The *post-hoc* analyses for this study revealed the statistical power to exceed 0.99 for the detection of differences between the fast and slow evolvers using the "slight delay" and "extended delay" bins, and the ~~rTTP-SRI~~rTTPIE index.

Ex vivo infarct assessment and correlation with MRI

In a subset of dogs (n = 6: 4 fast evolvers and 2 slow evolvers) after euthanasia, the brain was removed to histologically quantify the infarct volume using TTC. Overall, there was an excellent correlation between the final ADC-thresholded and the TTC-defined infarct volume ($R^2 = 0.99$) with a slope of 0.96 (data not shown).

Discussion

During human ELVO, the rate of infarct growth is determined by a combination of factors such as genetic background, demographics, physiological parameters, and other conditions that may influence collateral blood flow and ischemic tolerance [5, 38]. A key finding of our study was that the dog ELVO model, similar to monkeys [19], is characterized by variability in the ischemic stroke evolution that closely mimics the clinical scenario [38]. This phenomenon, in conjunction with the ability to study endovascular approaches to recanalization, renders the dog ELVO model as highly relevant to study novel therapeutic approaches in interventional research. Importantly, we show that voxel-wise analyses of PWI images allow to predict whether animals were fast or slow evolvers already on the first PWI scan obtained approximately 30 min after MCA occlusion.

Perfusion is a critical biological mechanism that reflects the delivery of oxygen and essential nutrients to tissue via blood flow. MR-based PWI has the potential to measure brain perfusion in acute stroke subjects and provide treatment options that may significantly affect the clinical outcome. DSC-MRI, compared to other PWI techniques like dynamic contrast-enhanced (DCE)-MRI and arterial-spin labeling (ASL), offers faster scan times to get a quick measurement of transit time with whole brain coverage, which can be critical in driving treatment decisions with a limited time window [83]. The deconvolved PWI parameters derived from DSC-MRI such as CBF, CBV, and MTT, have been considered to be more reliable in detecting tissue at risk of infarction due to the use of an arterial input function (AIF), which takes into account any variations in physiological and injection conditions [84, 85]. However, the AIF shape is susceptible to errors due to several factors such as motion artifacts and partial volume effects among others.[86, 87] Non-deconvolved PWI parameters derived from DSC-MRI such as TTP and BAT, on the other hand, do not require the measurement of an AIF and are derived directly from the tissue concentration time curve without any deconvolution.

TTP has been suggested to rapidly identify tissue at risk of infarction (penumbral tissue) and predict infarct size and growth in stroke patients [73, 75, 76, 88-91]. Thresholds of TTP delay (TTP > 4 s best identifying penumbral flow) [54, 72-76, 88, 92] were used to determine the volume of tissue that would become viable or that were at risk to progress to infarct. These TTP thresholds have been compared with ^{15}O-water positron emission tomography (PET) studies and validated using ^{15}O-water PET-derived CBF threshold of <20 ml/100 g/min, which serves as the “gold standard” for detecting penumbral tissue in ischemic stroke [57, 74-76, 92, 93]. In this study, we expanded the

role of TTP maps to assess the *extent* of critically hypoperfused brain tissue as well as to predict the *rate* of ~~stroke~~infarct evolution.

TTP maps have been generated in several different ways in clinical and animal studies over the last couple of decades. TTP map calculations have mainly been reported using three different methods where: 1.) TTP was defined as the time difference in peak intensity and the BAT [85, 94]; 2.) TTP was defined as the time from bolus injection to peak intensity [53, 54, 76, 95]; and 3.) TTP maps were generated using a normalization by subtracting a mean contralateral ROI of the unaffected hemisphere [54, 71-73, 75]. Since the latter method using normalization of the TTP map reduces AIF dependency (by lowering variability due to factors such as injection rate, catheter size, and cardiac output among others) and performs as well as deconvolved parameters in infarct prediction [57, 85, 86, 96], we used rTTP maps in this study to perform the histogram binning.

Histogram binning of rTTP maps successfully classified the animals into fast and slow evolvers based on the infarct growth rate observed in the ADC maps. The “slight delay” and “extended delay” bins in the histogram clearly distinguished between the fast and slow evolvers, which is numerically evident using the ~~rTTP-SRI~~rTTPIE index. Utilizing the rTTP map binning scheme promises to be useful in prospectively determining whether an animal will progress as a fast or slow evolver – a major advantage when studying novel therapeutics as it would allow to control for variability in infarct progression as part of the randomization scheme.

Limitations

One limitation from our analysis was that only two types of evolvers (fast and slow) were distinguishable using the rTTP analysis. If the ~~rTTP-SRI~~rTTPIE index value equaled close to one, then that would correspond to having approximately equal number of voxels in the “slight delay” and “extended delay” histogram bins of the rTTP maps, which would make it difficult to assign the animal as a fast or slow evolver. In that case, an “intermediate evolver” designation maybe more appropriate. The rTTP analysis to predict fast and slow evolvers was done retrospectively, which requires prospective confirmation of these preliminary findings. There was a notable variation in animal age and weight related to the different strains of dogs included into our retrospective analysis. However, we did not find any significant age and weight difference between fast and slow evolvers, assuaging concerns of major confounding and may in fact indicate broad applicability of our results. During the course of this proof-of-concept study, histology was not performed in all dogs for confirmation of the ADC thresholded infarct volume. However, in our past experience, the selected ADC threshold is highly concordant with histology [27, 28].

Conclusion

The canine model of embolic stroke resulting in the occlusion of the MCA results in both slow and fast infarct evolution. Preliminary evidence demonstrates that infarct evolution pattern can be determined immediately after clot placement using perfusion-weighted MRI. These data support more robust preclinical assessment of complex, multimodal acute stroke therapies.

Compliance with Ethical Standards

Conflict of Interest

Dr. Henninger is supported by K08NS091499 from the National Institute of Neurological Disorders and Stroke of the National Institutes of Health~~.~~ (NIH). The content is solely the responsibility of the authors and does not necessarily represent the official views of the ~~National Institutes of Health.~~NIH. Dr. Henninger serves on the advisory board of Omniox, Inc. and serves as consultant to Astrocyte Pharmaceuticals, Inc. Dr. Gounis has been a consultant on a fee-per-hour basis for Cerenovus, Imperative Care, Mivi Neurosciences, Phenox, Route 92 Medical, Stryker Neurovascular; holds stock in Imperative Care and Neurogami; and has received research support from the NIH, the United States – Israel Binational Science Foundation, Anaconda, Cerenovus, Ceretrieve, Cook Medical, Gentuity, Imperative Care, InNeuroCo, Magneto, Microvention, Medtronic Neurovascular, MIVI Neurosciences, Neuravi, Neurogami, Philips Healthcare, Rapid Medical, Route 92 Medical, Stryker Neurovascular, Syntheon, and the Wyss Institute. All authors declare that they have no potential conflicts of interest in regard to the research, authorship, and publication of this paper.

Ethical Approval

All animal research procedures were performed as approved by the Institutional Animal Care and Use Committee (IACUC) of the University of Massachusetts Medical School (Worcester, MA, USA). This article does not contain any studies with human participants performed by any of the authors.

Author Contribution Statement

The concept of study was developed by Matthew Gounis, Nils Henninger, Johannes Boltze, and Ajit Puri. Robert King and Matthew Gounis performed the animal experiments and collected the imaging data. Olivia Brooks performed data analysis. Mohammed Salman Shazeeb developed the image analysis pipeline, performed image analysis, and wrote the manuscript. Robert King also performed image analysis. Mathew Gounis, Nils Henninger, Johannes Boltze, and Robert King made significant edits to the manuscript for intellectual content. All authors read and approved the final manuscript.

Supplementary Information

None

References

1. Saver JL, Goyal M, Bonafe A, Diener HC, Levy EI, Pereira VM et al. Stent-retriever thrombectomy after intravenous t-PA vs. t-PA alone in stroke. N Engl J Med. 2015;372(24):2285-95. doi:10.1056/NEJMoa1415061.
2. Jovin TG, Chamorro A, Cobo E, de Miquel MA, Molina CA, Rovira A et al. Thrombectomy within 8 hours after symptom onset in ischemic stroke. N Engl J Med. 2015;372(24):2296-306. doi:10.1056/NEJMoa1503780.
3. Campbell BC, Mitchell PJ, Kleinig TJ, Dewey HM, Churilov L, Yassi N et al. Endovascular therapy for ischemic stroke with perfusion-imaging selection. N Engl J Med. 2015;372(11):1009-18. doi:10.1056/NEJMoa1414792.

4. Blanc R, Redjem H, Ciccio G, Smajda S, Desilles JP, Orng E et al. Predictors of the Aspiration Component Success of a Direct Aspiration First Pass Technique (ADAPT) for the Endovascular Treatment of Stroke Reperfusion Strategy in Anterior Circulation Acute Stroke. Stroke. 2017;48(6):1588-93. doi:10.1161/strokeaha.116.016149.
5. Mikati AG, Mandelbaum M, Sapnar S, Puri AS, Silver B, Goddeau RP, Jr. et al. Impact of Leukoaraiosis Severity on the Association of Time to Successful Reperfusion with 90-Day Functional Outcome After Large Vessel Occlusion Stroke. Transl Stroke Res. 2019. doi:10.1007/s12975-019-00703-0.
6. Bang OY, Goyal M, Liebeskind DS. Collateral Circulation in Ischemic Stroke: Assessment Tools and Therapeutic Strategies. Stroke. 2015;46(11):3302-9. doi:10.1161/strokeaha.115.010508.
7. Shuaib A, Butcher K, Mohammad AA, Saqqur M, Liebeskind DS. Collateral blood vessels in acute ischaemic stroke: a potential therapeutic target. Lancet Neurol. 2011;10(10):909-21. doi:10.1016/s1474-4422(11)70195-8.
8. Winship IR, Armitage GA, Ramakrishnan G, Dong B, Todd KG, Shuaib A. Augmenting collateral blood flow during ischemic stroke via transient aortic occlusion. J Cereb Blood Flow Metab. 2014;34(1):61-71. doi:10.1038/jcbfm.2013.162.
9. Henninger N, Fisher M. Stimulating circle of Willis nerve fibers preserves the diffusion-perfusion mismatch in experimental stroke. Stroke. 2007;38(10):2779-86. doi:10.1161/strokeaha.107.485581.
10. Shin HK, Nishimura M, Jones PB, Ay H, Boas DA, Moskowitz MA et al. Mild induced hypertension improves blood flow and oxygen metabolism in transient focal cerebral ischemia. Stroke. 2008;39(5):1548-55. doi:10.1161/strokeaha.107.499483.
11. Terpolilli NA, Kim SW, Thal SC, Kataoka H, Zeisig V, Nitzsche B et al. Inhalation of nitric oxide prevents ischemic brain damage in experimental stroke by selective dilatation of collateral arterioles. Circ Res. 2012;110(5):727-38. doi:10.1161/circresaha.111.253419.
12. Bratane BT, Cui H, Cook DJ, Bouley J, Tymianski M, Fisher M. Neuroprotection by freezing ischemic penumbra evolution without cerebral blood flow augmentation with a postsynaptic density-95 protein inhibitor. Stroke. 2011;42(11):3265-70. doi:10.1161/strokeaha.111.618801.

13. Hill MD, Martin RH, Mikulis D, Wong JH, Silver FL, Terbrugge KG et al. Safety and efficacy of NA-1 in patients with iatrogenic stroke after endovascular aneurysm repair (ENACT): a phase 2, randomised, double-blind, placebo-controlled trial. Lancet Neurol. 2012;11(11):942-50. doi:10.1016/s1474-4422(12)70225-9.

14. Sun HS, Doucette TA, Liu Y, Fang Y, Teves L, Aarts M et al. Effectiveness of PSD95 inhibitors in permanent and transient focal ischemia in the rat. Stroke. 2008;39(9):2544-53. doi:10.1161/strokeaha.107.506048.

15. Fisher M, Saver JL. Future directions of acute ischaemic stroke therapy. Lancet Neurol. 2015;14(7):758-67. doi:10.1016/s1474-4422(15)00054-x.

16. Bacigaluppi M, Comi G, Hermann DM. Animal models of ischemic stroke. Part two: modeling cerebral ischemia. Open Neurol J. 2010;4:34-8. doi:10.2174/1874205x01004020034.

17. Jahan R, Stewart D, Vinters HV, Yong W, Vinuela F, Vandeberg P et al. Middle cerebral artery occlusion in the rabbit using selective angiography: application for assessment of thrombolysis. Stroke. 2008;39(5):1613-5. doi:10.1161/STROKEAHA.107.507376.

18. Wey HY, Kroma GM, Li J, Leland MM, Jones L, Duong TQ. MRI of perfusion-diffusion mismatch in non-human primate (baboon) stroke: a preliminary report. Open Neuroimag J. 2011;5:147-52. doi:10.2174/1874440001105010147.

19. Zhang X, Tong F, Li CX, Yan Y, Kempf D, Nair G et al. Temporal evolution of ischemic lesions in nonhuman primates: a diffusion and perfusion MRI study. PLoS One. 2015;10(2):e0117290. doi:10.1371/journal.pone.0117290.

20. Hill NC, Millikan CH, Wakim KG, Sayre GP. Studies in cerebrovascular disease. VII Experimental production of cerebral infarction by intracarotid injection of homologous blood clot: preliminary report. Mayo Clin Proc. 1955;30(26):625-33.

21. Molinari GF. Experimental cerebral infarction. I. Selective segmental occlusion of intracranial arteries in the dog. Stroke. 1970;1(4):224-31.

22. Rink C, Christoforidis G, Abduljalil A, Kontzialis M, Bergdall V, Roy S et al. Minimally invasive neuroradiologic model of preclinical transient middle cerebral artery occlusion in canines. Proc Natl Acad Sci U S A. 2008;105(37):14100-5. doi:10.1073/pnas.0806678105.

23. Purdy PD, Devous MD, Sr., Batjer HH, White CL, 3rd, Meyer Y, Samson DS. Microfibrillar collagen model of canine cerebral infarction. Stroke. 1989;20(10):1361-7.
24. Harris AD, Kosior JC, Ryder RC, Andersen LB, Hu WY, Hudon M et al. MRI of ischemic stroke in canines: applications for monitoring intraarterial thrombolysis. J Magn Reson Imaging. 2007;26(6):1421-8. doi:10.1002/jmri.21189.
25. Shaibani A, Khawar S, Shin W, Cashen TA, Schirf B, Rohany M et al. First results in an MR imaging--compatible canine model of acute stroke. AJNR Am J Neuroradiol. 2006;27(8):1788-93.
26. Ahmed AS, Zellerhoff M, Strother CM, Pulfer KA, Redel T, Deuerling-Zheng Y et al. C-arm CT measurement of cerebral blood volume: an experimental study in canines. AJNR Am J Neuroradiol. 2009;30(5):917-22.
27. van der Bom IMJ, Mehra M, Walvick RP, Chueh J-Y, Gounis MJ. Quantitative evaluation of c-arm CT CBV in a canine model of ischemic stroke. AJNR Am J Neuroradiol. 2011;33:353-8.
28. Brooks OW, King RM, Nossek E, Marosfoi M, Caroff J, Chueh JY et al. A canine model of mechanical thrombectomy in stroke. J Neurointerv Surg. 2019. doi:10.1136/neurintsurg-2019-014969.
29. Anderson WD, Kubicek W. The vertebral-basilar system of dog in relation to man and other mammals. Am J Anat. 1971;132(2):179-88. doi:10.1002/aja.1001320205.
30. Wells AJ, Vink R, Blumbergs PC, Brophy BP, Helps SC, Knox SJ et al. A surgical model of permanent and transient middle cerebral artery stroke in the sheep. PLoS One. 2012;7(7):e42157. doi:10.1371/journal.pone.0042157.
31. Boltze J, Forschler A, Nitzsche B, Waldmin D, Hoffmann A, Boltze CM et al. Permanent middle cerebral artery occlusion in sheep: a novel large animal model of focal cerebral ischemia. J Cereb Blood Flow Metab. 2008;28(12):1951-64. doi:10.1038/jcbfm.2008.89.
32. Platt SR, Holmes SP, Howerth EW, Duberstein KJJ, Dove CR, Kinder HA et al. Development and characterization of a Yucatan miniature biomedical pig permanent middle cerebral artery occlusion stroke model. Exp Transl Stroke Med. 2014;6(1):5. doi:10.1186/2040-7378-6-5.

33. Mehra M, Henninger N, Hirsch JA, Chueh J, Wakhloo AK, Gounis MJ. Preclinical acute ischemic stroke modeling. J Neurointerv Surg. 2012;4(4):307-13. doi:10.1136/neurintsurg-2011-010101.
34. Herrmann AM, Meckel S, Gounis MJ, Kringe L, Motschall E, Mulling C et al. Large animals in neurointerventional research: A systematic review on models, techniques and their application in endovascular procedures for stroke, aneurysms and vascular malformations. J Cereb Blood Flow Metab. 2019;39(3):375-94. doi:10.1177/0271678x19827446.
35. Kang BT, Lee JH, Jung DI, Park C, Gu SH, Jeon HW et al. Canine model of ischemic stroke with permanent middle cerebral artery occlusion: clinical and histopathological findings. J Vet Sci. 2007;8(4):369-76.
36. Harris AD, Kosior RK, Chen HS, Andersen LB, Frayne R. Evolution of hyperacute stroke over 6 hours using serial MR perfusion and diffusion maps. J Magn Reson Imaging. 2009;29(6):1262-70. doi:10.1002/jmri.21763.
37. Christoforidis GA, Vakil P, Ansari SA, Dehkordi FH, Carroll TJ. Impact of Pial Collaterals on Infarct Growth Rate in Experimental Acute Ischemic Stroke. AJNR Am J Neuroradiol. 2017;38(2):270-5. doi:10.3174/ajnr.A5003.
38. Rocha M, Jovin TG. Fast Versus Slow Progressors of Infarct Growth in Large Vessel Occlusion Stroke: Clinical and Research Implications. Stroke. 2017;48(9):2621-7. doi:10.1161/strokeaha.117.017673.
39. Wheeler HM, Mlynash M, Inoue M, Tipirnini A, Liggins J, Bammer R et al. The growth rate of early DWI lesions is highly variable and associated with penumbral salvage and clinical outcomes following endovascular reperfusion. Int J Stroke. 2015;10(5):723-9. doi:10.1111/ijs.12436.
40. Ribo M, Molina CA, Cobo E, Cerda N, Tomasello A, Quesada H et al. Association Between Time to Reperfusion and Outcome Is Primarily Driven by the Time From Imaging to Reperfusion. Stroke. 2016;47(4):999-1004. doi:10.1161/strokeaha.115.011721.
41. Copen WA, Rezai Gharai L, Barak ER, Schwamm LH, Wu O, Kamalian S et al. Existence of the diffusion-perfusion mismatch within 24 hours after onset of acute stroke: dependence on proximal arterial occlusion. Radiology. 2009;250(3):878-86. doi:10.1148/radiol.2503080811.

42. Marchal G, Beaudouin V, Rioux P, de la Sayette V, Le Doze F, Viader F et al. Prolonged persistence of substantial volumes of potentially viable brain tissue after stroke: a correlative PET-CT study with voxel-based data analysis. Stroke. 1996;27(4):599-606.
43. Schellinger PD, Jansen O, Fiebach JB, Heiland S, Steiner T, Schwab S et al. Monitoring intravenous recombinant tissue plasminogen activator thrombolysis for acute ischemic stroke with diffusion and perfusion MRI. Stroke. 2000;31(6):1318-28.
44. Wu O, Koroshetz WJ, Ostergaard L, Buonanno FS, Copen WA, Gonzalez RG et al. Predicting tissue outcome in acute human cerebral ischemia using combined diffusion- and perfusion-weighted MR imaging. Stroke. 2001;32(4):933-42.
45. Ostergaard L, Sorensen AG, Chesler DA, Weisskoff RM, Koroshetz WJ, Wu O et al. Combined diffusion-weighted and perfusion-weighted flow heterogeneity magnetic resonance imaging in acute stroke. Stroke. 2000;31(5):1097-103.
46. Schaefer PW, Hunter GJ, He J, Hamberg LM, Sorensen AG, Schwamm LH et al. Predicting cerebral ischemic infarct volume with diffusion and perfusion MR imaging. AJNR Am J Neuroradiol. 2002;23(10):1785-94.
47. Wheeler HM, Mlynash M, Inoue M, Tipirneni A, Liggins J, Zaharchuk G et al. Early diffusion-weighted imaging and perfusion-weighted imaging lesion volumes forecast final infarct size in DEFUSE 2. Stroke. 2013;44(3):681-5. doi:10.1161/strokeaha.111.000135.
48. Olivot JM, Mlynash M, Thijs VN, Purushotham A, Kemp S, Lansberg MG et al. Geography, structure, and evolution of diffusion and perfusion lesions in Diffusion and perfusion imaging Evaluation For Understanding Stroke Evolution (DEFUSE). Stroke. 2009;40(10):3245-51. doi:10.1161/strokeaha.109.558635.
49. Rordorf G, Koroshetz WJ, Copen WA, Cramer SC, Schaefer PW, Budzik RF, Jr. et al. Regional ischemia and ischemic injury in patients with acute middle cerebral artery stroke as defined by early diffusion-weighted and perfusion-weighted MRI. Stroke. 1998;29(5):939-43.
50. Le Bihan D, Breton E, Lallemand D, Grenier P, Cabanis E, Laval-Jeantet M. MR imaging of intravoxel incoherent motions: application to diffusion and perfusion in neurologic disorders. Radiology. 1986;161(2):401-7. doi:10.1148/radiology.161.2.3763909.

51. Wesbey GE, Moseley ME, Ehman RL. Translational molecular self-diffusion in magnetic resonance imaging. II. Measurement of the self-diffusion coefficient. Invest Radiol. 1984;19(6):491-8.
52. Moseley ME, Cohen Y, Mintorovitch J, Chileuitt L, Shimizu H, Kucharczyk J et al. Early detection of regional cerebral ischemia in cats: comparison of diffusion- and T2-weighted MRI and spectroscopy. Magn Reson Med. 1990;14(2):330-46.
53. Copen WA, Schaefer PW, Wu O. MR perfusion imaging in acute ischemic stroke. Neuroimaging Clin N Am. 2011;21(2):259-83. doi:10.1016/j.nic.2011.02.007.
54. Neumann-Haefelin T, Wittsack HJ, Wenserski F, Siebler M, Seitz RJ, Modder U et al. Diffusion- and perfusion-weighted MRI. The DWI/PWI mismatch region in acute stroke. Stroke. 1999;30(8):1591-7.
55. Albers GW. Expanding the window for thrombolytic therapy in acute stroke. The potential role of acute MRI for patient selection. Stroke. 1999;30(10):2230-7.
56. Rivers CS, Wardlaw JM, Armitage PA, Bastin ME, Carpenter TK, Cvoro V et al. Do acute diffusion- and perfusion-weighted MRI lesions identify final infarct volume in ischemic stroke? Stroke. 2006;37(1):98-104. doi:10.1161/01.STR.0000195197.66606.bb.
57. Takasawa M, Jones PS, Guadagno JV, Christensen S, Fryer TD, Harding S et al. How reliable is perfusion MR in acute stroke? Validation and determination of the penumbra threshold against quantitative PET. Stroke. 2008;39(3):870-7. doi:10.1161/strokeaha.107.500090.
58. Baird AE, Lovblad KO, Dashe JF, Connor A, Burzynski C, Schlaug G et al. Clinical correlations of diffusion and perfusion lesion volumes in acute ischemic stroke. Cerebrovasc Dis. 2000;10(6):441-8. doi:10.1159/000016105.
59. Barber PA, Parsons MW, Desmond PM, Bennett DA, Donnan GA, Tress BM et al. The use of PWI and DWI measures in the design of "proof-of-concept" stroke trials. J Neuroimaging. 2004;14(2):123-32.
60. Butcher K, Parsons M, Baird T, Barber A, Donnan G, Desmond P et al. Perfusion thresholds in acute stroke thrombolysis. Stroke. 2003;34(9):2159-64. doi:10.1161/01.str.0000086529.83878.a2.

61. Parsons MW, Barber PA, Chalk J, Darby DG, Rose S, Desmond PM et al. Diffusion- and perfusion-weighted MRI response to thrombolysis in stroke. Ann Neurol. 2002;51(1):28-37.
62. Parsons MW, Yang Q, Barber PA, Darby DG, Desmond PM, Gerraty RP et al. Perfusion magnetic resonance imaging maps in hyperacute stroke: relative cerebral blood flow most accurately identifies tissue destined to infarct. Stroke. 2001;32(7):1581-7.
63. Rohl L, Geday J, Ostergaard L, Simonsen CZ, Vestergaard-Poulsen P, Andersen G et al. Correlation between diffusion- and perfusion-weighted MRI and neurological deficit measured by the Scandinavian Stroke Scale and Barthel Index in hyperacute subcortical stroke (< or = 6 hours). Cerebrovasc Dis. 2001;12(3):203-13. doi:10.1159/000047705.
64. Rohl L, Ostergaard L, Simonsen CZ, Vestergaard-Poulsen P, Andersen G, Sakoh M et al. Viability thresholds of ischemic penumbra of hyperacute stroke defined by perfusion-weighted MRI and apparent diffusion coefficient. Stroke. 2001;32(5):1140-6.
65. Rose SE, Chalk JB, Griffin MP, Janke AL, Chen F, McLachan GJ et al. MRI based diffusion and perfusion predictive model to estimate stroke evolution. Magn Reson Imaging. 2001;19(8):1043-53.
66. Rose SE, Janke AL, Griffin M, Finnigan S, Chalk JB. Improved prediction of final infarct volume using bolus delay-corrected perfusion-weighted MRI: implications for the ischemic penumbra. Stroke. 2004;35(11):2466-71. doi:10.1161/01.STR.0000145199.64907.5a.
67. Ueda T, Yuh WT, Maley JE, Quets JP, Hahn PY, Magnotta VA. Outcome of acute ischemic lesions evaluated by diffusion and perfusion MR imaging. AJNR Am J Neuroradiol. 1999;20(6):983-9.
68. Yoo AJ, Verduzco LA, Schaefer PW, Hirsch JA, Rabinov JD, Gonzalez RG. MRI-based selection for intra-arterial stroke therapy: value of pretreatment diffusion-weighted imaging lesion volume in selecting patients with acute stroke who will benefit from early recanalization. Stroke. 2009;40(6):2046-54. doi:10.1161/strokeaha.108.541656.
69. Mlynash M, Lansberg MG, De Silva DA, Lee J, Christensen S, Straka M et al. Refining the definition of the malignant profile: insights from the DEFUSE-EPITHET pooled data set. Stroke. 2011;42(5):1270-5. doi:10.1161/strokeaha.110.601609.

70. Kakuda W, Lansberg MG, Thijs VN, Kemp SM, Bammer R, Wechsler LR et al. Optimal definition for PWI/DWI mismatch in acute ischemic stroke patients. J Cereb Blood Flow Metab. 2008;28(5):887-91. doi:10.1038/sj.jcbfm.9600604.
71. Kim S, Kang M, Choi S, Kim DW. Mismatch of delayed perfusion volume between TTP and Tmax map of perfusion MRI. Clin Imaging. 2016;40(1):63-7. doi:10.1016/j.clinimag.2015.10.005.
72. Thomalla GJ, Kucinski T, Schoder V, Fiehler J, Knab R, Zeumer H et al. Prediction of malignant middle cerebral artery infarction by early perfusion- and diffusion-weighted magnetic resonance imaging. Stroke. 2003;34(8):1892-9. doi:10.1161/01.str.0000081985.44625.b6.
73. Wouters A, Christensen S, Straka M, Mlynash M, Liggins J, Bammer R et al. A Comparison of Relative Time to Peak and Tmax for Mismatch-Based Patient Selection. Front Neurol. 2017;8:539. doi:10.3389/fneur.2017.00539.
74. Zaro-Weber O, Moeller-Hartmann W, Siegmund D, Kandziora A, Schuster A, Heiss WD et al. MRI-based mismatch detection in acute ischemic stroke: Optimal PWI maps and thresholds validated with PET. J Cereb Blood Flow Metab. 2017;37(9):3176-83. doi:10.1177/0271678x16685574.
75. Sobesky J, Zaro Weber O, Lehnhardt FG, Hesselmann V, Thiel A, Dohmen C et al. Which time-to-peak threshold best identifies penumbral flow? A comparison of perfusion-weighted magnetic resonance imaging and positron emission tomography in acute ischemic stroke. Stroke. 2004;35(12):2843-7. doi:10.1161/01.STR.0000147043.29399.f6.
76. Reimer J, Montag C, Schuster A, Moeller-Hartmann W, Sobesky J, Heiss WD et al. Is Perfusion MRI without Deconvolution Reliable for Mismatch Detection in Acute Stroke? Validation with 15O-Positron Emission Tomography. Cerebrovasc Dis. 2018;46(1-2):16-23. doi:10.1159/000490424.
77. Ogata T, Nagakane Y, Christensen S, Ma H, Campbell BC, Churilov L et al. A topographic study of the evolution of the MR DWI/PWI mismatch pattern and its clinical impact: a study by the EPITHET and DEFUSE Investigators. Stroke. 2011;42(6):1596-601. doi:10.1161/strokeaha.110.609016.

78. Lansberg MG, Straka M, Kemp S, Mlynash M, Wechsler LR, Jovin TG et al. MRI profile and response to endovascular reperfusion after stroke (DEFUSE 2): a prospective cohort study. Lancet Neurol. 2012;11(10):860-7. doi:10.1016/s1474-4422(12)70203-x.
79. Short CE. Principles & Practice of Veterinary Anesthesia. Williams & Wilkins; 1987.
80. Bratane BT, Bastan B, Fisher M, Bouley J, Henninger N. Ischemic lesion volume determination on diffusion weighted images vs. apparent diffusion coefficient maps. Brain Res. 2009;1279:182-8. doi:10.1016/j.brainres.2009.05.002.
81. Kang BT, Jang DP, Gu SH, Lee JH, Jung DI, Lim CY et al. MRI features in a canine model of ischemic stroke: correlation between lesion volume and neurobehavioral status during the subacute stage. Comp Med. 2009;59(5):459-64.
82. Faul F, Erdfelder E, Lang AG, Buchner A. G*Power 3: a flexible statistical power analysis program for the social, behavioral, and biomedical sciences. Behav Res Methods. 2007;39(2):175-91.
83. Jahng GH, Li KL, Ostergaard L, Calamante F. Perfusion magnetic resonance imaging: a comprehensive update on principles and techniques. Korean J Radiol. 2014;15(5):554-77. doi:10.3348/kjr.2014.15.5.554.
84. Calamante F, Thomas DL, Pell GS, Wiersma J, Turner R. Measuring cerebral blood flow using magnetic resonance imaging techniques. J Cereb Blood Flow Metab. 1999;19(7):701-35. doi:10.1097/00004647-199907000-00001.
85. Perthen JE, Calamante F, Gadian DG, Connelly A. Is quantification of bolus tracking MRI reliable without deconvolution? Magn Reson Med. 2002;47(1):61-7.
86. Christensen S, Mouridsen K, Wu O, Hjort N, Karstoft H, Thomalla G et al. Comparison of 10 perfusion MRI parameters in 97 sub-6-hour stroke patients using voxel-based receiver operating characteristics analysis. Stroke. 2009;40(6):2055-61. doi:10.1161/strokeaha.108.546069.
87. Calamante F. Arterial input function in perfusion MRI: a comprehensive review. Prog Nucl Magn Reson Spectrosc. 2013;74:1-32. doi:10.1016/j.pnmrs.2013.04.002.
88. Motta M, Ramadan A, Hillis AE, Gottesman RF, Leigh R. Diffusion-perfusion mismatch: an opportunity for improvement in cortical function. Front Neurol. 2014;5:280. doi:10.3389/fneur.2014.00280.

89. Wittsack HJ, Ritzl A, Fink GR, Wenserski F, Siebler M, Seitz RJ et al. MR imaging in acute stroke: diffusion-weighted and perfusion imaging parameters for predicting infarct size. Radiology. 2002;222(2):397-403. doi:10.1148/radiol.2222001731.
90. Grandin CB, Duprez TP, Smith AM, Oppenheim C, Peeters A, Robert AR et al. Which MR-derived perfusion parameters are the best predictors of infarct growth in hyperacute stroke? Comparative study between relative and quantitative measurements. Radiology. 2002;223(2):361-70. doi:10.1148/radiol.2232010673.
91. Drier A, Tourdias T, Attal Y, Sibon I, Mutlu G, Lehericy S et al. Prediction of subacute infarct size in acute middle cerebral artery stroke: comparison of perfusion-weighted imaging and apparent diffusion coefficient maps. Radiology. 2012;265(2):511-7. doi:10.1148/radiol.12112430.
92. Zaro-Weber O, Moeller-Hartmann W, Heiss WD, Sobesky J. MRI perfusion maps in acute stroke validated with 15O-water positron emission tomography. Stroke. 2010;41(3):443-9. doi:10.1161/strokeaha.109.569889.
93. Werner P, Saur D, Zeisig V, Ettrich B, Patt M, Sattler B et al. Simultaneous PET/MRI in stroke: a case series. J Cereb Blood Flow Metab. 2015;35(9):1421-5. doi:10.1038/jcbfm.2015.158.
94. Martel AL, Allder SJ, Delay GS, Morgan PS, Moody AA. Perfusion MRI of infarcted and noninfarcted brain tissue in stroke: a comparison of conventional hemodynamic imaging and factor analysis of dynamic studies. Invest Radiol. 2001;36(7):378-85.
95. Hartmann A, Driesen A, Lautenschlager IE, Scholz VB, Schmidt MJ. Quantitative analysis of brain perfusion in healthy dogs by means of magnetic resonance imaging. Am J Vet Res. 2016;77(11):1227-35. doi:10.2460/ajvr.77.11.1227.
96. Meijs M, Christensen S, Lansberg MG, Albers GW, Calamante F. Analysis of perfusion MRI in stroke: To deconvolve, or not to deconvolve. Magn Reson Med. 2016;76(4):1282-90. doi:10.1002/mrm.26024.

Figure Legends

Fig. 1 Placement of an autologous clot in the middle cerebral artery (MCA) of the dog. (**a**) Digital Subtraction Angiography (DSA) prior to clot placement is shown. The arrows indicate the location of the MCA (**b**) Total MCA occlusion is shown in DSA post-clot placement. The dashed arrows depict the original course of the MCA, which is now absent. (**c**) Time-of-flight (ToF) MRI shows an open internal carotid artery (ICA) and an occluded MCA.

Fig. 2 Flowchart of image analysis. Apparent diffusion coefficient (ADC) and time-to-peak (TTP) maps were generated from diffusion-weighted imaging (DWI) and perfusion-weighted imaging (PWI), respectively. ADC maps were used to calculate the final ~~stroke~~infarct volume. The entire brain in TTP maps was normalized with respect to a representative area on the contralateral side of the ~~stroke~~infarct region to generate relative TTP (rTTP) maps. rTTP maps were registered with ADC maps to count the voxels within the ~~stroke~~infarct volume. All voxels within the ADC-defined lesion were binned into one of four categories in the rTTP map. The total size of each bin, across the entire lesion volume, was used to predict the rate of ~~stroke~~infarct evolution.

Fig. 3 Representative animal from the fast evolver group (Animal #4 from Table 1). (**a**) Final diffusion-weighted imaging (DWI) image showing the total extent of the infarct as a hyperintense region. (**b**) Apparent diffusion coefficient (ADC) map showing a hypointense region indicating the extent of infarct. The red line on the scale bar indicates the intensity

level of the infarct region. (**c**) Post-mortem triphenyltetrazolium chloride (TTC) staining showing the final histological ~~stroke~~infarct size. Scale bar: 10 mm. (**d**) Relative time-to-peak (rTTP) map derived from perfusion-weighted imaging (PWI) images. The color intensity of the infarct area voxels indicate an elevated intensity at or above the 20-s delay. Digital Subtraction Angiography (DSA) is shown in early (**e**) and delayed phase (**f**), which denote a lack of collaterals in the right hemisphere. The arrows indicate the location of the clot.

Fig. 4 Representative animal from the slow evolver group (Animal #1 from Table 1). (**a**) Final diffusion-weighted imaging (DWI) image showing the total extent of the infarct as a hyperintense region. (**b**) Apparent diffusion coefficient (ADC) map showing a hypointense region indicating the extent of infarct. The red line on the scale bar indicates the intensity level of the infarct region. (**c**) Post-mortem triphenyltetrazolium chloride (TTC) staining showing the final histological ~~stroke~~infarct size. Scale bar: 10 mm. (**d**) Relative time-to-peak (rTTP) map derived from perfusion-weighted imaging (PWI) images. The area of occlusion is seen only slightly elevated with a few voxels above the 20-s delay. Digital Subtraction Angiography (DSA) is shown in early (**e**) and delayed phase (**f**), which highlights the impact of the collaterals in the left hemisphere. The arrows indicate the location of the clot.

Fig. 5 Quantification of fast and slow evolvers using diffusion-weighted imaging (DWI) apparent diffusion coefficient (ADC) maps and perfusion-weighted imaging (PWI) time-to-peak (TTP) maps. (**a**) Ischemic core evolution as derived by ADC-thresholded maps

and dichotomized to fast (orange) versus slow (blue) evolvers are shown. Based on lesion growth rate, animals were divided into fast (>50% total volume within 2 h) and slow (<50% total volume within 2 h) evolver groups. The plot shows the progression of slow and fast evolvers with the greatest difference occurring at about 2 h. Individual growth curves are shown for each animal in lighter shade. Error bars indicate SEM. (**b**) Correlation plot is shown indicating the agreement of infarct volumes between the final DWI image and the TTP map generated from the initial PWI images (R^2 = 0.99). The dotted lines indicate 95% confidence level. (**c**) Histogram binning from rTTP maps for fast and slow evolvers are shown. The voxels in the "slight delay" bin (4−8 s) of fast evolvers are significantly fewer compared to that of slow evolvers (**p < 0.0001). The dashed line near the left axis of the plot shows a cutoff at ~34%, which distinguishes between the fast and slow evolvers in the "slight delay" bin. The voxels in the "extended delay" bin (19+ s) of fast evolvers are significantly more compared to that of slow evolvers (*p = 0.0013). The dashed line near the right axis of the plot shows a cutoff at ~42%, which ~~distinguish s~~distinguishes between the fast and slow evolvers in the "extended delay" bin. The two middle bins of "moderate delay" (9−13 s) and "long delay" (14−18 s) did not show any significant differences between the slow and fast evolvers. Error bars indicate SEM.

We thank the reviewers for their comments and have included the responses to their queries below in red. In addition, we rephrased terms like stroke volume and stroke rate with infarct volume and infarct evolution rate throughout the manuscript. We also updated the funding/conflict of interest information.

Reviewer #1: In this study, the authors used DWI and PWI technology to divide ELVO dogs into fast evolvers and slow evolvers increasing the scientific rigor, which enabling more robust study design for follow-up interventional research.

Some points need to be pay attention to:

1. In the figure 3 and figure 4, why were the infarcts located in the diferent side? Generally we select the same side of infarts in animal model for the rigor of the study.

Thank you for pointing this out. The choice of left versus right side for infarct modeling was based on the angiographic features of the cervical ICA. We selected the larger ICA with sufficient non-tortuous origin for placement of the catheter. We revised our methods section to include this information as follows: "The side of clot injection was selected on the basis of the larger diameter and length of non-tortuous cervical ICA for delivery of this relatively large catheter."

2. The authors should add a scale to figure 3C and figure 4C.

A scale has been added to the figures and the figure caption has been edited to include the scale information. We apologize for the oversight.

3. How is it defined in terms of distinguishing between slow and fast evolvers were ~34% for the "slight delay" and ~42% for the "extended delay" bins

The definition was based on the spread of the data points in the fast and slow evolver categories in Fig 5C for the “slight delay” and “extended delay” bins. ~34% and ~42% were approximately the halfway values between the boundary data points of the fast and slow evolvers. Hence, the rTTPIE (rTTP infarct evolution) index was used as the more quantitative measure to designate fast and slow evolvers. The Results section has been revised to now read as follows: “the respective cutoff marks to distinguish between slow and fast evolvers were ~34% for the “slight delay” and ~42% for the “extended delay” bins based on the minimal distance (halfway point) between the boundary points of each category.

4. The authors should give a calculation formula or specific method of rTTP and compare the affected area with the mirror image area.

Thank you for the suggestion. As requested, we added this information to the revised methods section as follows: "To obtain a relative TTP (rTTP) map, TTP maps were normalized by subtracting the mean TTP derived from a contralateral region of interest (ROI; positioned in the periventricular area of the unaffected hemisphere in the mid-brain region) from the absolute TTP in each voxel using the following equation:

$$rTTP_{map} = TTP_{map} - \frac{1}{n}\sum_{i=1}^{n}(ROI_{contralateral})_i$$

where *n* is the total number of voxels in the contralateral ROI. "

5. Why is there such a big difference in the selection of the age of the animals in the group, and the weight of the older animals in the aging state is very low, which may be an unstable factor in this study.

The variability in animal age and weight relates to the different strains of dogs used in this study. However, size and age of the animal were not statistically different between the slow and fast evolver groups (see Table 2) assuaging concerns that these factors biased our results. Nevertheless, your point is well taken and we revised our limitation to briefly address this issue as follows: “There was a notable variation in animal age and weight related to the different strains of dogs included into our retrospective analysis. However, we did not find any significant age and weight difference between fast and slow evolvers, assuaging concerns of major confounding and may in fact indicate broad applicability of our results.”

Reviewer #2: An excellent experimental model to hopefully get closer to answering the topical question of reasons for the gap between recanalized patients and those with good clinical outcome. The canine model is a close replica of the human circle of willis and hence can be a good experimental model to assess novel therapeutic targets in the future. Well designed study with MCA occlusion model. Good demonstration of the hypothesis of selecting out animals with slow progression of infarct volume vs fast progression. The utilization of MRI every 30 minutes to closely follow infarct evolution is a robust mechanism to study the phenomenon in question. This model can be applied to further prospective evaluation to validate further and then can be utilized to study interventions with novel therapeutic targets.

We appreciate the enthusiasm of the reviewer and agree that this model will be applicable to prospective studies to validate therapeutic interventions.

Figure 1

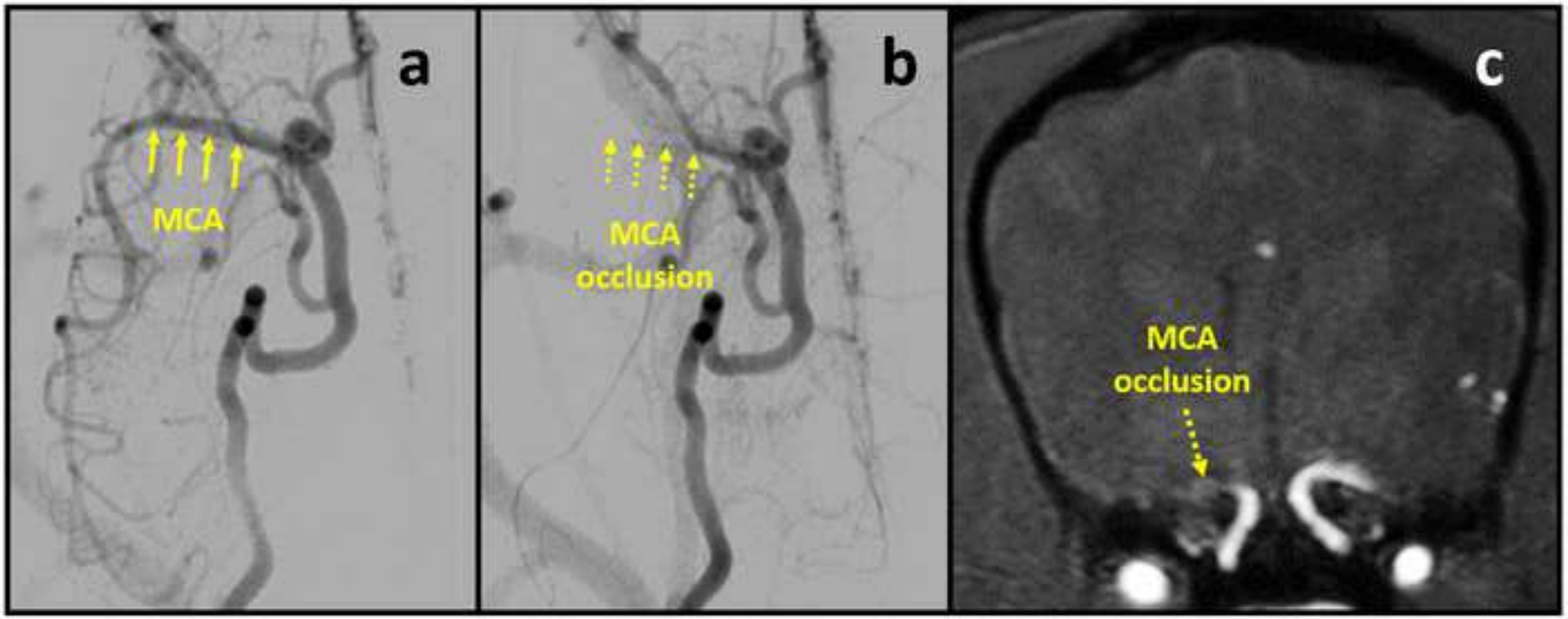

Figure 2

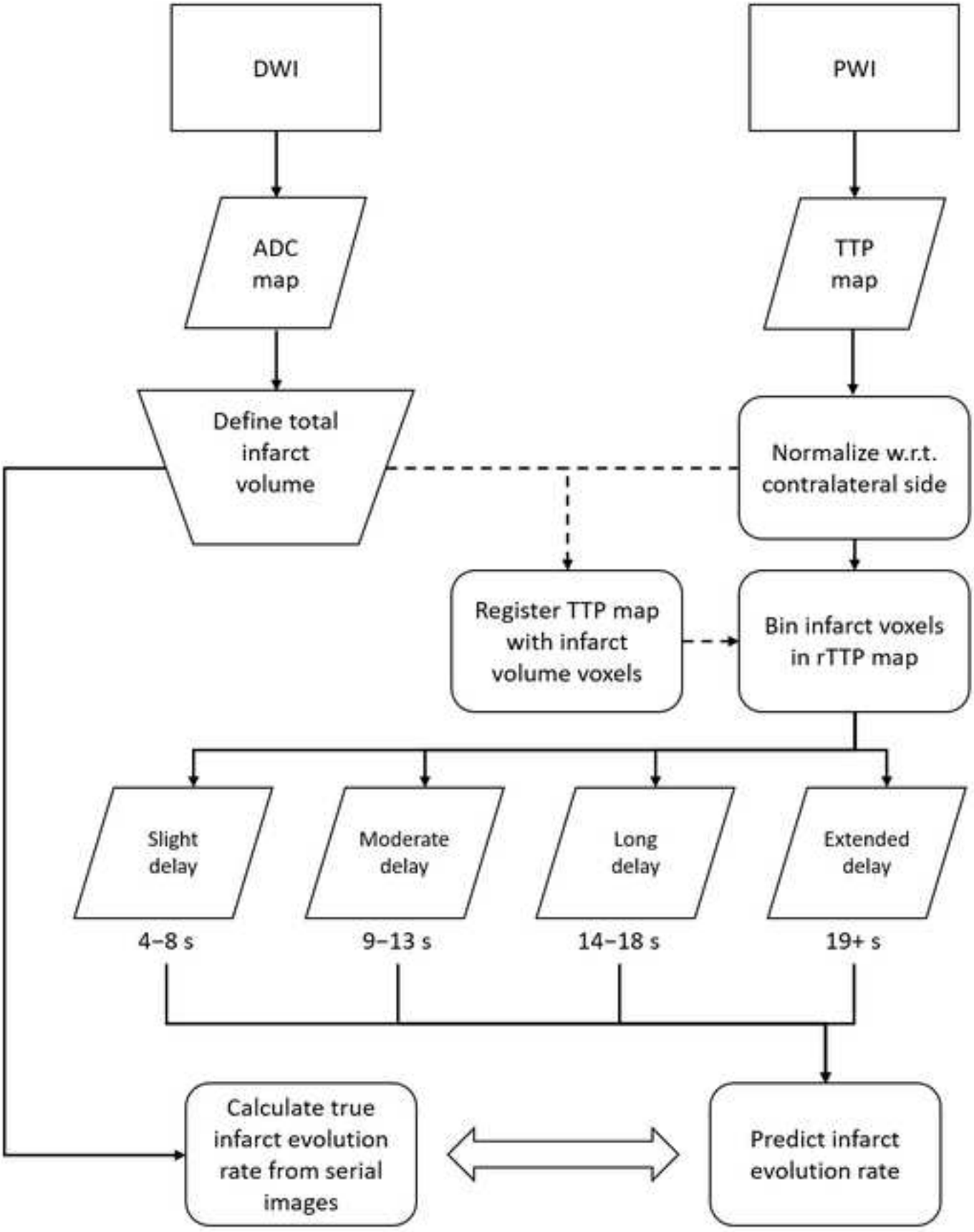

Figure 3

Click here to access/download;Figure;Fig3.tif

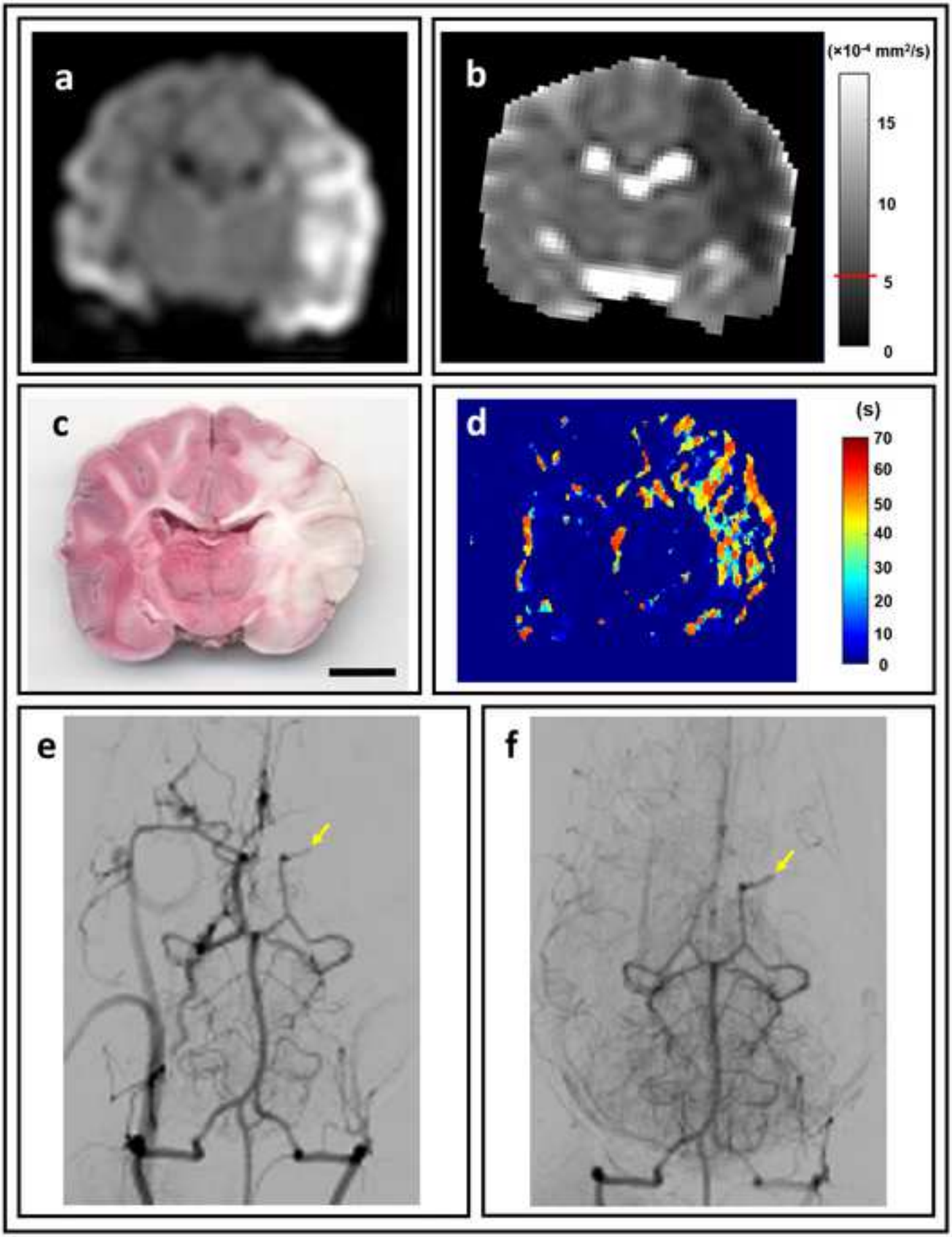

Figure 4

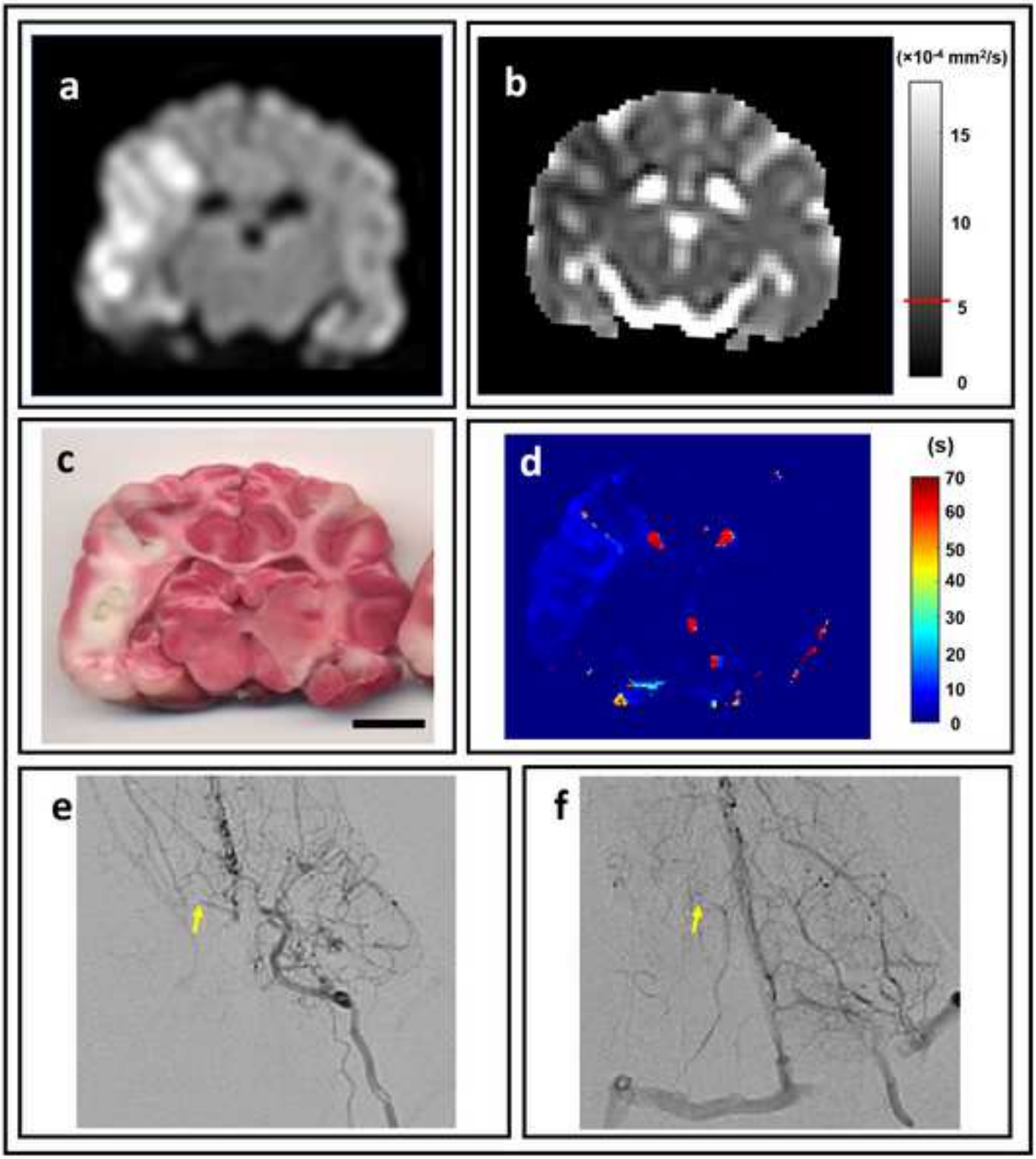

Figure 5

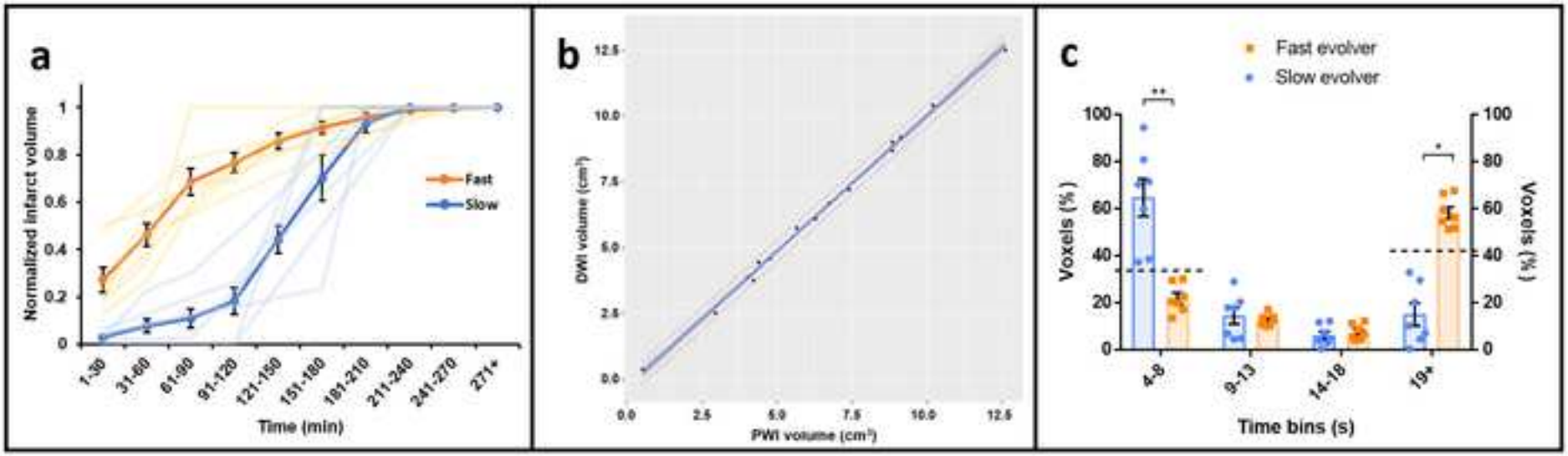

Tables

Table 1. Demographic data and infarct evolution rate of subjects

Animal ID	Age (months)	Sex	Weight (kg)	Infarct evolution rate	rTTPIE[a] index
Animal 1	7.0	Female	21.2	Slow	0.003
Animal 2	6.5	Male	14.7	Fast	2.615
Animal 3	17.0	Male	8.9	Slow	0.125
Animal 4	8.0	Female	21.3	Fast	5.043
Animal 5	16.5	Male	9.3	Fast	2.676
Animal 6	6.75	Female	22.8	Slow	0.074
Animal 7	15.5	Male	13.0	Slow	0.882
Animal 8	16.0	Male	12.5	Slow	0.099
Animal 9	10.5	Female	23.9	Fast	2.634
Animal 10	10.0	Female	23.4	Fast	1.721
Animal 11	26.0	Male	8.2	Slow	0.286
Animal 12	36.0	Female	10.1	Fast	1.908
Animal 13	30.5	Female	9.8	Slow	0.767
Animal 14	32.5	Female	9.4	Fast	3.896
Mean ± SD	17.1 ± 10.2		14.9 ± 6.2		1.62 ± 1.59

[a] rTTPIE – relative time-to-peak infarct evolution

Table 2. Statistical summary of fast and slow evolvers

	Fast Evolvers	Slow Evolvers	*p* value
Sex (% female)	71	43	0.32
Age (months)	17.1 ± 12.1	17.0 ± 8.9	0.98
Weight (kg)	16.0 ± 6.7	13.8 ± 5.9	0.52
rTTPIE[a] index	2.93 ± 1.17	0.32 ± 0.36	0.0001

[a] rTTPIE – relative time-to-peak infarct evolution